Title

Pentavalent Curium, Berkelium, and Californium in Nitrate Complexes: Extending Actinide Chemistry and Oxidation States

Journal

Inorganic Chemistry, 57(15)

ISSN

0020-1669

Authors

Kovács, Attila

Dau, Phuong D

Marçalo, Joaquim

et al.

Publication Date

2018-08-06

DOI

10.1021/acs.inorgchem.8b01450

Peer reviewed

Pentavalent Curium, Berkelium and Californium in Nitrate Complexes: Extending Actinide Chemistry and Oxidation States

Attila Kovács[1,*], Phuong D. Dau[2], Joaquim Marçalo[3], John K. Gibson[2,*]

[1]European Commission, Joint Research Centre, P.O. Box 2340, 76125 Karlsruhe, Germany

[2]Chemical Sciences Division, Lawrence Berkeley National Laboratory, Berkeley, CA, 94720 USA

[3]Centro de Ciências e Tecnologias Nucleares & Centro de Química Estrutural, Instituto Superior Técnico, Universidade de Lisboa, 2695-066 Bobadela LRS, Portugal

[*]Corresponding authors: Attila.KOVACS@ec.europa.eu; jkgibson@lbl.gov

Abstract

Pentavalent actinyl nitrate complexes $An^{V}O_2(NO_3)_2^-$ were produced by elimination of two NO_2 from $An^{III}(NO_3)_4^-$ for An = Pu, Am, Cm, Bk and Cf. Density functional theory (B3LYP) and relativistic multireference (CASPT2) calculations confirmed the $AnO_2(NO_3)_2^-$ as $An^{V}O_2^+$ actinyl moieties coordinated by nitrates. Computations of alternative $An^{III}O_2(NO_3)_2^-$ and $An^{IV}O_2(NO_3)_2^-$ revealed significantly higher energies. Previous computations for bare AnO_2^+ indicated $An^{V}O_2^+$ for An = Pu, Am, Cf and Bk, but $Cm^{III}O_2^+$: electron donation from nitrate ligands has here stabilized the first Cm^{V} complex, $Cm^{V}O_2(NO_3)_2^-$. Structural parameters and bonding analyses indicate increasing An-NO_3 bond covalency from Pu to Cf, in accord with principles for actinide separations. Atomic ionization energies effectively predict relative stabilities of oxidation states; more reliable energies are needed for the actinides.

Introduction

The range of accessible oxidation states (OSs) of an element is fundamental to its chemistry. In particular, high OSs provide an assessment of the propensity, and ultimately the ability, of valence electrons to become engaged in chemical bonding. Until recently, the highest known OS in the entire periodic table was VIII, such as in the stable and volatile molecules RuO_4 and OsO_4. The OS IX was finally realized in the gas-phase complex IrO_4^+,[1] but neither this moiety nor this highest OS have been isolated in condensed phase.[1-2] The appearance of distinctive and otherwise inaccessible chemistry in gas-phase species, such as Ir^{IX} in IrO_4^+, is generally attributed to isolation of a moiety that would otherwise be highly reactive with neighbor species in condensed phases.[3] For example, gas-phase PaO_2^{2+}, which comprises *formally* Pa^{VI}, has been synthesized but it activates even dihydrogen to yield atomic H and $PaO_2(OH)^{2+}$ in which the stable discrete Pa^V OS state is recovered.[4] In view of its gas-phase reactivity, there is scant chance of isolating PaO_2^{2+} in condensed phase. Another example of a distinctively high OS accessible (so far) only in the gas phase is Pr^V in PrO_2^+ and NPrO,[5-6] this being the only known pentavalent lanthanide.

The early actinides yield ultimate OSs, from Ac^{III} to Np^{VIII}, that correspond to engagement of all valence electrons in chemical bonding to yield an empty $5f^0$ valence electron shell.[7] After Np, the highest accessible actinide OSs, from Pu^{VII} to lower OSs beyond Pu, have one or more chemically unengaged valence 5f electron(s), as the nuclear charge increases and energies of the 5f orbitals decrease. The transition from chemical participation of all 5f valence electrons in ubiquitous U^{VI}, to participation of only two valence electrons in prevalent No^{II},[8] distinguishes the actinides from the lanthanides for which the relatively low energy of the valence 4f orbitals results in only a few OSs above trivalent.[9] The gas-phase molecular ions BkO_2^+ and CfO_2^+ were recently synthesized and their OSs computed as Bk^V and Cf^V, which was an advancement beyond oxidation state IV for these elements and extended the distinctive actinyl(V) dioxo moieties into the second half of the actinide series.[10] It is notable that the computed oxidation state in ground-state CmO_2^+ is not Cm^V but rather Cm^{III}, which reflects the limited stabilities of OSs above III for the actinides after Am.[10]

A primary goal of the work reported here is to assess stabilities of OSs, particularly the pentavalent OS, of the actinides Cm, Bk and Cf. These elements represent the transition from the early actinides that exhibit higher OS, including Am^{VI} and possibly also Am^{VII},[11] to the latest actinides, Es through Lr, that have been definitively identified only in the An^{II} and/or

An^{III} OS. The meagre realm of OSs for the late actinides may not be entirely due to intrinsic chemistry because synthetic efforts for these elements have been very limited due to scarcity and short half-lives of available synthetic isotopes. Cm, Bk and Cf are the heaviest actinides available as isotopes that are both sufficiently abundant (>10 μg) and long-lived (>100 d) for application of some conventional experimental approaches with relatively moderate procedural modifications. A gas-phase synthesis approach to achieve high OSs is nitrate decomposition, whereby an anionic NO_3 ligand coordinated to a metal is converted to an oxygen atom ligand with release of neutral NO_2. If the created ligand is O^{2-}, which replaces the disrupted NO_3^- ligand, then the metal OS has been increased by one. However, if an increased metal OS is inadequately stable, then the created ligand may instead be radical $O^{\bullet}$ (formally O^-) with retention of the original metal OS. This approach was previously employed to oxidize $An^{III}(NO_3)_4^-$ to $An^{IV}O(NO_3)_3^-$.[12] We here extend this synthetic method to seek oxidation beyond An^{IV}, to potential An^V in $AnO_2(NO_3)_2^-$, with particular targets being Cm^V, Bk^V and Cf^V. The pentavalent OS were recently assigned for BkO_2^+ and CfO_2^+,[10] and an objective here is to extend and characterize these OSs in more complex coordination environments that include nitrate ligands. It was previously predicted that ground-state CmO_2^+ does not comprise Cm^V but rather that the structure is the peroxide $Cm(O_2)^+$ in which the oxidation state is Cm^{III}.[10] We here assess the effect of nitrate coordination on the stability of Cm^V in the CmO_2^+ core of $CmO_2(NO_3)_2^-$, concluding that the higher OS is stabilized by nitrate coordination. The geometric and electronic properties of the synthesized complexes were assessed by density functional theory (DFT) and multireference CASPT2 calculations. The computational results affirm the assignments of pentavalent actinide OSs in the observed $AnO_2(NO_3)_2^-$ complexes and provide insights into the bonding in these complexes. The calculations furthermore indicate a general increase in the covalency of An-nitrate bonding interactions from An = Pu to An = Cf. Stabilities of high actinide OS are evaluated in relation to pertinent atomic ionization energies for removal of one or more electrons, with the conclusion that the chemical property of OS is generally well predicted from these fundamental atomic properties.

Experimental Section

Caution! The ^{242}Pu, ^{243}Am, ^{245}Cm, ^{249}Bk and ^{249}Cf isotopes employed in this work are highly radioactive and must be handled only with proper authorization and using established radiological safety protocols.

The general experimental approach of electrospray ionization (ESI) synthesis and collision induced dissociation (CID) fragmentation of metal nitrates to yield oxide nitrates has been described previously.[12] Unique aspects of such types of ESI and gas-phase ion chemistry experiments employing a few micrograms of ^{249}Bk or ^{249}Cf have also been reported.[10] The following stock solutions were used here to prepare the ESI solutions: 8 mM $^{242}PuO_2(ClO_4)_2$ at pH = 1; 0.67 mM $^{243}AmO_2(NO_3)_3^-$ at pH = 1; 0.40 µM ^{249}Cf and ~0.02 µM ^{245}Cm (~5% ^{245}Cm relative to ^{249}Cf) in 100 mM HCl; 10 mM $CeBr_3$ in water; 10 mM $PrBr_3$ in water; 10 mM $NdBr_3$ in water; 10 mM $TbCl_3$ in water; and 100 mM HNO_3. The ^{249}Bk was supplied as $BkCl_3$, which was dissolved in ~80% ethanol and ~20% water to yield a 10 mM stock solution. The final ESI solutions contained 100 µM actinide or lanthanide and 10 mM HNO_3 in a mixture of ~80% ethanol and ~20% water. ^{249}Bk beta decays with a half-life of ~320 d to nearly isobaric ^{249}Cf. At the time the experiments were performed there was ~7% ^{249}Cf progeny relative to ^{249}Bk parent; the results for the pure Cf sample confirm that the observations for 93%Bk/7%Cf reveal the chemistry of the dominant Bk component. ^{249}Cf alpha decays with a half-life of ~351 y to ^{245}Cm, which isotopes are easily resolved by mass spectrometry. At the time the experiments were performed, there was ~5% ^{245}Cm progeny relative to ^{249}Cf parent; the amount of ^{245}Cm was sufficient for isolation and gas-phase chemistry of both Cm and Cf nitrate complexes from this sample.

The ESI mass spectrometry experiments were performed using an Agilent 6340 quadrupole ion trap mass spectrometer (QIT/MS) with MS^n CID capabilities. Additionally, ions in the trap can undergo ion/molecule reactions for a fixed time at ~300K. The source region of the QIT/MS is inside of a radiological-containment glove box, as described in detail elsewhere.[13] In high-resolution mode, the instrument has a detection range of 50 – 2200 *m/z* and a resolution of $M/\Delta M \approx 3000$. Mass spectra were acquired using the following instrumental parameters: solution flow rate, 60 µl/min; nebulizer gas pressure, 12 psi; capillary voltage and current, 4000 V, 40.283 nA; end plate voltage offset and current, -500 V, 775 nA; dry gas flow rate, 3 l/min; dry gas temperature, 325 °C; capillary exit, -300.0 V; skimmer, -47.6 V; octopole 1 and 2 DC, -10.40 V and -1.80 V; octopole RF amplitude, 300.0 V_{pp}; lens 1 and 2, 15.0 V and 100.0 V; trap drive, 64.3. High-purity nitrogen gas for nebulization and drying in the ion transfer capillary was supplied from the boil-off of a liquid nitrogen Dewar. As has been discussed elsewhere, the background water pressure in the ion trap is estimated as ~10^{-6} Torr;[14] reproducibility of hydration rates of $UO_2(OH)^+$ confirmed

that the background water pressure in the trap varied by less than ±5%.[15] The helium buffer gas pressure in the trap was constant at ~10^{-4} Torr.

Computational Details

The DFT computations were performed with the Gaussian09 suite of programs,[16] using the B3LYP exchange-correlation functional.[17-18] For the actinides the Stuttgart-Cologne small-core pseudopotentials (ECP60MWB[19]) were used in conjunction with 14s13p10d8f6g valence basis sets contracted to 10s9p5d4f3g (ECP60MWB_SEG[20]). For nitrogen and oxygen the correlation consistent aug-cc-pVTZ bases[21-22] were applied.

The computed model structures have a net charge of 1-. The spin multiplicities have been selected according to the number of expected unpaired electrons in the anions, i.e. gradually increasing from 3 to 7 for Pu to Cf. In order to ensure the proper value for this parameter, test calculations were also performed for models with the neighbouring lower and higher spin multiplicities. The different electronic structure resulted in several cases in different spatial symmetry. The minimum character of the obtained stationary points on the potential energy surface was confirmed in all cases by frequency analysis.

The topological analysis of the electron density distribution was performed by means of the AIMAll software.[23] The natural atomic charges were obtained by natural bond orbital (NBO) analysis[24] utilizing the NBO6.0 code.[25]

The relativistic multireference calculations were performed using the code MOLCAS 8.0.[26-27] The complete active space self-consistent field (CASSCF) method[28] was used to generate molecular orbitals and reference functions for subsequent multiconfigurational second-order perturbation theory calculations of the dynamic correlation energy (CASPT2)[29-30] with frozen 1s for O, and up to 4f for An.

In the CASSCF calculations, the scalar relativistic effects were taken into account using the second-order Douglas-Kroll-Hess (DKH2) Hamiltonian.[31-32] The ground-state molecular geometries were optimized at the spin-orbit-free CASPT2 level using numerical gradients. The initial geometries in these optimizations were those obtained by the DFT calculations. We performed also test calculations starting from structures with lower symmetry. In most cases they confirmed the symmetries of the DFT ground states (vide infra).

All electron basis sets of atomic natural orbital type, developed for relativistic calculations (ANO-RCC) with the Douglas-Kroll-Hess Hamiltonian[31-32] were used for the complexes with An = Pu - Cm. Basis sets with contraction schemes of

26s23p17d13f5g3h/9s8p6d5f2g1h[33] and 14s9p4d3f2g/4s3p2d1f[34] were used for the actinides and the main group elements (N and O), respectively, corresponding to TZP quality.

ANO-RCC basis sets are not available for the heavy actinides Bk and Cf. For these two actinides the same relativistic small-core Stuttgart-Cologne pseudopotentials[19] were used as in the Gaussian calculations (accordingly, these CASPT2 calculations were performed without the DKH2 Hamiltonian). For N and O Dunning's correlation consistent cc-pVTZ basis sets[21] have been used (denoted as TZ).

The active space was constructed on the basis of state-averaged test calculations using 5 roots. Based on the observed occupations[35] and cost considerations, the following active spaces (electron/orbital) were applied in the calculations of the symmetric (D_{2h}, C_{2v}, C_2) structures: 11/13, 12/13, 13/13, 16/15 and 17/15 were used for An = Pu, Am, Cm, Bk and Cf, respectively. The 13 active orbitals of the Pu, Am and Cm complexes included four two-electron An=O bonding orbitals, and seven orbitals with major An 5f contribution. The rest were strongly mixed orbitals (including among others An 6d), for which the mentioned test calculations indicated reasonable occupations. In the case of Bk and Cf, two additional strongly mixed orbitals were affected by static correlation, therefore we used 15 active orbitals in these latter active spaces.

For CASPT2 geometry optimization of C_1 structures of the lower oxidation state Cf and Bk complexes, the TZ basis set proved to be too expensive. Therefore, we applied the cc-pVDZ basis sets for N and O (denoted as DZ). For the same reason, the above large active spaces were reduced by removing three two-electron orbitals with mainly An=O bonding contributions. These active spaces contained 10 and 11 electrons in 12 orbitals for the Bk and Cf complexes, respectively. The final relative energies were obtained by subsequent single-point energy calculations at the CASPT2/TZ level utilizing C_1 symmetry for all the involved species.

The z axis corresponds to the axis of the C_2 symmetry operation in the C_{2v} structures (cf. Scheme 1). This defines the magnetic quantum numbers of the 6d and 5f orbitals given in the Tables.

Results and discussion

The experimental results are first presented, along with a discussion as to the rationale for inferring that the produced $AnO_2(NO_3)_2^-$ complexes likely comprise pentavalent An^V. The subsequent sections provide computational assessments of the ground-state pentavalent $An^VO_2(NO_3)_2^-$ complexes, as well as the alternative higher-energy trivalent An^{III} and

tetravalent An^{IV} structures, and computational evaluations of the characteristics of the ground-state $An^{V}O_2(NO_3)_2^-$ complexes. Finally, relationships between actinide reduction potentials, ionization energies and oxidation states, particularly the pentavalent oxidation state, are evaluated.

1. Synthesis of actinyl nitrate complexes

It was previously found that the lanthanide (Ln) complexes $Ln^{III}(NO_3)_4^-$ that were produced by ESI exhibit NO_2 elimination upon endothermic CID to yield $LnO(NO_3)_3^-$, according to reaction 1.[12] For most lanthanides, an oxidation state of Ln^{III} is assigned in the produced monoxide trinitrate complexes, each with a Ln-O• radical-like single bond that is susceptible to exothermic hydrolysis ion/molecule reaction 2 (IMR 2) to yield $Ln^{III}(OH)(NO_3)_3^-$. However, for Ln = Ce, Pr, Nd and Tb—the lanthanides with the lowest, and thus least favourable, $Ln^{IV/III}$ reduction potentials—the assigned oxidation state in the $LnO(NO_3)_3^-$ complexes is Ln^{IV} as substantiated by the resistance of their strong and saturated Ln=O double bonds to disruption by reaction 2. Reaction 1 was also found to occur for actinides An = Pu, Am and Cm. Because the $An^{IV/III}$ reduction potentials for these An are lower than for Pr, Nd or Tb, it was surmised that the oxidation states are An^{IV} with An=O double bonds, and thus correctly predicted that IMR 2 should not occur.

$M^{III}(NO_3)_4^- \rightarrow MO(NO_3)_3^- + NO_2$ M = Ln or An (1) CID / $\Delta E > 0$

$MO(NO_3)_3^- + H_2O \rightarrow M^{III}(OH)(NO_3)_3^- + OH$ (2) IMR / $\Delta E < 0$

In the present work, CID mass spectra were acquired for $Ln^{III}(NO_3)_4^-$ where Ln = Ce, Pr, Nd and Tb. As the results in Figure 1 reveal, the dominant primary products of these CID reactions were the $LnO(NO_3)_3^-$ species produced according to reaction 1, as reported previously.[12] Under the CID conditions employed here—i.e., a nominal instrumental fragmentation energy of 0.5 V—a distinct and reproducible peak in the CID mass spectrum due to $PrO_2(NO_3)_2^-$ appeared. This peak, evident in Figure 1, is due to secondary CID reaction 3 for the particular case of M = Ln = Pr. Notably, this secondary product did not appear in the CID spectra of other $Ln(NO_3)_4^-$, specifically not for Ln = Ce, Nd or Tb (see Fig. 1). Because the only known pentavalent lanthanide is Pr(V) in PrO_2^+ and NPrO,[5-6] the distinctive occurrence of CID reaction 3 for M = Pr is likely due to the existence of this stable praseodymium dioxo cation moiety in the nitrate complex, which may be represented as $(PrO_2^+)(NO_3^-)_2$ with an overall net charge of -1. In the previous study it was mentioned that some $LnO_2(NO_3)_2^-$ were produced by CID of $Ln(NO_3)_4^-$ but this observation was not elaborated and there was no indication that Pr was distinctive in this behaviour.[12]

$MO(NO_3)_3^- \rightarrow MO_2(NO_3)_2^- + NO_2$ (3) CID / $\Delta E > 0$

The distinctive appearance of the $PrO_2(NO_3)_2^-$ lanthanide complex that evidently reveals the particular stability of Pr^V motivated extending this approach to transuranium actinides to assess stabilities of pentavalent An. Gas-phase processes such as reactions 1-3 are particularly well-suited for experimental studies of scarce and highly radioactive actinides such Cm, Bk and Cf, which are difficult to isolate and characterize in condensed phases. CID mass spectra of $An^{III}(NO_3)_4^-$ for An = Pu, Am, Cm, Bk and Cf are shown in Fig. 2. The CID conditions were the same for these five $An^{III}(NO_3)_4^-$ and for the four $Ln^{III}(NO_3)_4^-$ for which results are shown in Fig. 1 (Ln = Ce, Pr, Nd, Tb). As reported previously for An = Pu, Am and Cm,[12] and also now found here for An = Bk and Cf, primary CID reaction 1 yields $AnO(NO_3)_3^-$, which are formally $(AnO^{2+})(NO_3^-)_3$. The oxidation state in the AnO^{2+} moieties was previously assigned as An(IV) for Pu, Am and Cm.[12] Given that the (estimated) IV/III reduction potentials for Bk (1.7 V) and Cf (3.2 V),[7] are lower than that for Nd (4.6 V)[9] that is considered to have oxidation state Nd^{IV} in $NdO(NO_3)_3^-$,[12] it is inferred that the oxidation states in the $(AnO^{2+})(NO_3^-)_3$ complexes are similarly Bk^{IV} and Cf^{IV} as is substantiated by their resistance to hydrolysis during the CID experiments to yield $An^{III}(OH)(NO_3)_3^-$.[12]

A particularly notable result in Figure 2 is the appearance of $AnO_2(NO_3)_2^-$ for each of the studied actinides, An = Pu, Am, Cm, Bk and Cf. Comparison of these results with those for Pr and other Ln shown in Figure 1—along with the knowledge that the oxidation state is Pr(V) in bare PrO_2^+ and also presumably in the PrO_2^+ core of $PrO_2(NO_3)_2^-$—suggests pentavalent actinides in the dioxo dinitrate anion product complexes. The actinyl(V) cations PuO_2^+ and AmO_2^+ are stable in solution and solid complexes.[36] In accord with the well-established stabilities of these two actinyl moieties, the CID yields of $PuO_2(NO_3)_2^-$ and $AmO_2(NO_3)_2^-$ are particularly high. Although the CID abundances of $AnO_2(NO_3)_2^-$ for An = Cm, Bk and Cf were relatively minor—similar to the yield of $PrO_2(NO_3)_2^-$ under comparable conditions—these products were consistently and reproducibly observed. The computational results presented below affirm the inference that the five synthesized $AnO_2(NO_3)_2^-$ comprise actinyl(V) cores.

2. Spatial and electronic structure

The potential energy surface of the $AnO_2(NO_3)_2^-$ complexes was probed by DFT calculations in order to find the probable structures and most stable spin multiplicities, which were studied subsequently by the more expensive CASPT2 calculations. For the DFT

calculations the B3LYP exchange-correlation functional in conjunction with polarized triple-zeta valence basis set was selected, which level provided recently very good results for actinyl derivatives[37] and also generally for actinide compounds.[38]

The composition of the $AnO_2(NO_3)_2^-$ complexes implies symmetric (D_{2h}, C_{2v}) molecular geometries. In order to explore the flat potential energy surfaces of the title compounds, we probed several less symmetric initial structures for the geometry optimization in the DFT and in some CASPT2 calculations.

The found ground electronic states from the B3LYP calculations are listed in Table 1. Beyond the ground-state spin multiplicities the most stable states of the neighbouring spin multiplicities are also given.

Table 1. The most stable states of the probed spin multiplicities of $AnO_2(NO_3)_2^-$ complexes from B3LYP calculations.[a]

An	Spin	Symmetry	Irrep	ΔE
Pu	2	D_{2h}	n.a.	74.7
	4	D_{2h}	B_{1u}	0.0
	6	C_{2v}	B_1	244.6
Am	3	D_{2h}[b]	A	95.2
	5	D_{2h}	A_g	0.0
	7	C_{2v}	B_1	177.1
Cm	4	C_{2h}	B_u	129.3
	6	C_{2v}	A_1	0.0
	8	C_s	A"	86.4
Bk	5	D_{2h}	n.a.	124.0
	7	C_{2v}	B_2	0.0
	9	C_1	A	213.6
Cf	6	C_{2v}	A_2	0.0
	8	C_2	A	81.0
	10	C_1	A	375.8

[a]Spin means the spin multiplicity; Symmetry means the spatial symmetry of the optimized structure; Irrep means the irreducible representation of the given states. The computed relative energies (kJ/mol) refer to the ground electronic states.
[b]While the optimized structure has D_{2h} symmetry, the symmetry of the electronic state suffered from a break to C_2.

As shown by the large energy differences in Table 1, the ground-states multiplicities are straightforward for all five actinides covered in the present study. Noteworthy is the high symmetry of these ground-state structures: D_{2h} for Pu and Am, while C_{2v} for Cm, Bk and Cf. The spin multiplicities of the ground states increase gradually from Pu (4) to Bk (7), while a

turning point seems to appear at Cf (6). According to the analysis of the electronic and molecular structures (vide infra), all these ground states correspond to pentavalent An.

Table 2. Electronic structures of the ground states of $An^{V}O_2(NO_3)_2^-$ complexes from CASPT2 calculations.[a]

An	Spin	Symmetry	Irrep	Config	Population
Pu	4	D_{2h}	B_{1u}	91%	$5f_{1+}$, $5f_{1-}$, $5f_{2-}$
Am	5	D_{2h}	A_g	88%	$5f_0$, $5f_{1+}$, $5f_{1-}$, $5f_{2-}$
	5	C_{2v}	A_1	87%	$5f_0$, $5f_{1+}$, $5f_{1-}$, $5f_{2-}$
Cm	6	C_{2v}	A_1	85%	$5f_0$, $5f_{1+}$, $5f_{1-}$, $5f_{2+}$, $5f_{2-}$
Bk	7	C_{2v}	B_2	84%	$5f_0$, $5f_{1+}$, $5f_{1-}$, $5f_{2+}$, $5f_{2-}$, $5f_{3-}$
Cf	6	C_{2v}	A_2	85%	$5f_0$, $5f_{1-}$, $5f_{2-}$, $5f_{2+}$, $5f_{3-}$

[a]Spin means the spin multiplicity; Symmetry means the spatial symmetry of the optimized structure; Irrep means the irreducible representation of the given states; Config means the contribution of the main configuration state function in %.

Table 2 compiles the most important electronic characteristics of the ground states from CASPT2 calculations. These multireference calculations confirmed the ground-state spin multiplicities from DFT, and in most cases the symmetries of the ground-state structures too. The only exception was the $Am^{V}O_2(NO_3)_2^-$ complex, for which DFT predicted a D_{2h} global minimum structure, while the CASPT2 calculations converged to a C_{2v} one. The two structures have the same electron configuration (A_g and A_1 irreps in D_{2h} and C_{2v}, respectively, cf. Table 2) On the CASPT2 potential energy surface the D_{2h} structure (saddle-point) is only slightly (0.9 kJ/mol) higher in energy than the C_{2v} minimum. In the view of the accuracy of these calculations, this very small energy difference may not be relevant.

Another important information from Table 2 is the generally high contribution (over 84%) of the main configuration state function to the wavefunction. In these cases, the system can efficiently be estimated by density functional theory as shown by the present good performance of the used B3LYP level. The population of the 5f orbitals shows a systematic pattern in the $An^{V}O_2(NO_3)_2^-$ complexes based on the $5f_{1+}$, $5f_{1-}$, $5f_{2-}$ populations in $Pu^{V}O_2(NO_3)_2^-$. This pattern is extended by the population of $5f_0$ in $Am^{V}O_2(NO_3)_2^-$, then by $5f_{2+}$ in $Cm^{V}O_2(NO_3)_2^-$ and by the $5f_{3-}$ orbitals in the complexes of the late actinides. In the sextet $Cf^{V}O_2(NO_3)_2^-$, the singly-populated 5f orbitals lack $5f_{1+}$, which in this molecule is a doubly occupied non-bonding orbital.

3. Tri- and tetravalent An derivatives

During the search for the $An^{V}O_2(NO_3)_2^-$ (An = Bk, Cf) ground states from C_1 initial structures we located the most probable structures for these An^{IV} and An^{III} derivatives by

B3LYP/TZ and CASPT2/DZ geometry optimizations. The frequency calculations at the B3LYP level confirmed the minimum character of the presented structures on the respective potential energy surfaces. We discuss the Cf^{IV} and Cf^{III} species in detail, their structures depicted in two perspectives in Figure 3. All the geometry parameters together with those of related structures of the Bk^{IV} and Bk^{III} species are given in SI.

The structure of octet $Cf^{IV}O_2(NO_3)_2^-$ is close to C_2 symmetry, but it has a characteristic difference in the two Cf-O_{yl} (yl = 1, 1', cf. Scheme 1) bond distances: the one with 1.806 Å corresponds to a Cf=O double bond, while the other bond with a length of 2.145 Å is in agreement with a single Cf-O bond (CASPT2/DZ data, cf. Figure 3 top). This bonding scenario justifies the oxidation state IV for Cf in this species and C_1 symmetry for the structure. We note that a very similar octet $Cf^{V}O_2(NO_3)_2^-$ structure but with equivalent Cf-O_{yl} double bonds (in this way achieving C_2 symmetry) was also found by our CASPT2 calculations and the minimum character confirmed by B3LYP frequencies. It lies higher in energy by ca. 80 kJ/mol than the sextet $Cf^{V}O_2(NO_3)_2^-$ ground state (cf. Table 1).

The CASPT2/DZ geometry optimization predicted for $Cf^{III}O_2(NO_3)_2^-$ a structure with C_{2v} symmetry (Figure 3 bottom). The main structural feature is the peroxide O_2^{2-} group replacing the two O_{yl} oxygens of the higher oxidation-state forms. The O-O bond distance of 1.575 Å and the Cf-O_{peroxi} distances of 2.071 Å (corresponding to single Cf-O bonds) confirm the trivalent state of Cf in this molecule. We note that the Cf…NO_3^- distances are in good agreement with those in the $Cf^{V}O_2(NO_3)_2^-$ and $Cf^{IV}O_2(NO_3)_2^-$ structures suggesting that the character of the Cf…NO_3^- interaction is not substantially changed by the variation of the Cf oxidation state.

Table 3. Compilation of the found $AnO_2(NO_3)_2^-$ complexes with tri- and tetravalent Cf and Bk.[a]

An	Spin	Symmetry	ΔE(B3LYP)	ΔE(CASPT2)[b]
Cf^{IV}	8	C_1	80.1	96.4
Cf^{III}	6	C_2/C_{2v}[c]	33.5	134.1
Bk^{IV}	7	C_1	81.5	416.2
Bk^{III}	7	C_1	79.1	241.5
Bk^{III}	5	C_1	240.4	571.8

[a]Spin means the spin multiplicity; Symmetry means the spatial symmetry of the optimized structure; The computed relative energies (kJ/mol) refer to the pentavalent ground electronic states.
[b]Single-point CASPT2/TZ energies with respect to $An^{V}O_2(NO_3)_2^-$ forms calculated on the CASPT2/DZ geometries.
[c]The B3LYP/TZ geometry optimization resulted in a C_1 (though close to C_{2v}) structure.

The relative energies with respect to $An^{V}O_2(NO_3)_2^-$ (An = Cf, Bk) are shown in Table 3. The stabilities of the $Cf^{V}/Cf^{IV}/Cf^{III}$ and $Bk^{V}/Bk^{IV}/Bk^{III}$ oxidation states are important for understanding the results of our gas-phase experiments. Both the CASPT2 and B3LYP calculations predicted a considerable relative stability of the Cf^{V} and Bk^{V} states with respect to the lower-valent ones (the B3LYP level generally underestimating the relative energies compared to CASPT2). Hence our theoretical data confirm the assignment of the small peaks observed in the mass spectra of $CfO_2(NO_3)_2^-$ and $BkO_2(NO_3)_2^-$ to the pentavalent forms. For these two actinides the low-oxidation state complexes of Cf are closer in energy to $Cf^{V}O_2(NO_3)_2^-$ than those of Bk to $Bk^{V}O_2(NO_3)_2^-$.

4. Characteristics of the $An^{V}O_2(NO_3)_2^-$ ground states

The quantum chemical calculations uncovered some additional interesting features of the molecular properties of the title complexes. The CASPT2 geometry data of the $An^{V}O_2(NO_3)_2^-$ ground states compiled in Table 4 reflect how the characteristic geometrical properties vary with the increasing atomic number of An. (The B3LYP geometry data are in SI). The compilation of the ground states (and the following comparison) is extended to the lowest energy octet $Cf^{V}O_2(NO_3)_2^-$ structure, which is not the ground state, because it fits the trend of increasing spin multiplicities.

The variation of geometry is best reflected by the O_1-An-$O_{1'}$ and N-An-N angles decreasing from the value of 180.0° present in the D_{2h} Pu complex. The considerably smaller deformation of the O_1-An-$O_{1'}$ angle is consistent with the rigid character of the delocalized π bonding in the actinyl moiety in contrast to the more flexible ligands. The decreasing trend is going on gradually from Pu to octet Cf, though the changes between Bk and Cf are enhanced due to the change of symmetry from C_{2v} to C_2. We note that in spite of the considerably bent O_1-Cf-$O_{1'}$ angle (110.5°) the multiple bond character of the Cf-O_{yl} bonds did not change as indicated by the short Cf-O_{yl} bond distances. The sextet $CfO_2(NO_3)_2^-$ shows small differences compared to $BkO_2(NO_3)_2^-$ due to the same C_{2v} symmetry of the two molecules. The only striking change is the increased O_1-An-$O_{1'}$ angle for sextet $CfO_2(NO_3)_2^-$ relative to septet $BkO_2(NO_3)_2^-$.

The An-O_2/$O_{2'}$ distances (the average values in the case of C_{2v} are 2.495, 2.466, 2.422, and 2.402 Å for Am, Cm, Bk and Cf, respectively) show a consistent decrease from Am to sextet Cf. This implies strengthening bonding interactions between An and NO_3^- in this range of the actinide row. Interestingly, the strengthening bonding correlates with the bend of the

two NO_3^- ligands around An, the latter feature shown by the decrease of the N-An-N angle (cf. Table 4).

Table 4. Geometrical parameters[a] of the $An^{V}O_2(NO_3)_2^-$ complexes computed at the CASPT2 level.

Parameters	Pu	Am	Cm	Bk	Cf	Cf
Symmetry	D_{2h}	C_{2v}	C_{2v}	C_{2v}	C_{2v}	C_2
Spin	4	5	6	7	6	8
An-O_1	1.779	1.775	1.809	1.818	1.795	1.815
O_1-An-$O_{1'}$	180.0	178.5	174.8	164.8	169.1	110.5
An-O_2	2.487	2.483	2.453	2.385	2.376	2.374
An-$O_{2'}$	2.487	2.506	2.478	2.458	2.428	2.495
N-An-N	180.0	153.0	148.7	136.6	135.0	109.2
O_2-An-O_2	128.4	101.5	96.6	83.5	81.5	148.4
N-O_2	1.272	1.272	1.273	1.278	1.274	1.284
N-$O_{2'}$	1.272	1.272	1.273	1.269	1.272	1.266
N-O_3	1.225	1.227	1.225	1.219	1.220	1.218
O_2-N-$O_{2'}$	116.7	117.0	116.8	116.3	116.4	116.1
O_2-N-O_3	121.7	121.5	121.6	122.2	121.9	121.2
O_2-N-N-O_2	0.0	0.0	0.0	0.0	0.0	-73.9

[a]Bond distances are given in angstroms, bond angles in degrees. For the notation of atoms see Scheme 1.

The bonding between An and NO_3^- consists of a mixture of electrostatic and orbital interactions. Due to the considerable positive charge of An and the negative charge of the nitrate oxygens, the electrostatic attraction is very strong between the two moieties. The most favourable electrostatic interaction can be expected in the D_{2h} arrangement, where the NO_3^- ligands lie at the opposite sides of An. When the N-An-N angle is bent from this linear arrangement, repulsion can appear between the negatively charged nitrate oxygens, which approach one another upon bending. Therefore, the bent relative orientation of the NO_3^- ligands in the heavier An derivatives (the D_{2h} symmetry lowered to C_{2v}) is not favourable from the point of view of ionic bonding. Then, what can be the reason for the observed symmetry lowering?

We considered the possibility that the electron density distribution around the pentavalent An in AnO_2^+ is deformed and a local electron density concentration in the horizontal plane of AnO_2^+ enforces a bending of the NO_3^- ligands, like lone pairs do in main group compounds. This hypothesis, however, can be dismissed based upon the available information on the structure of AnO_2^+ ions. According to our present knowledge, based on multireference calculations on the light actinides An = Th – Cm, the ground state structure of

AnO_2^+ ions is linear.[38-39] A local charge concentration in the horizontal plane would bend the O-An-O angle in these ions.

The exclusion of an electrostatic origin of bending is further supported by the electron density map of the C_{2v} structure of $Cm^VO_2(NO_3)_2^-$ depicted in Figure 4. It demonstrates charge concentration on the oxygens (yellow), near neutral character of the nitrogens (green) while charge depletion around Cm. The maximum of charge depletion appears on the top (dark blue), which spatial region is left free after the downward bend of the NO_3^- ligands. Hence, there is no substantial electron density in this region, which would repulse the negatively charged nitrate oxygens and thus would force a bend.

Hence, after excluding the electrostatic origin of the C_{2v} structures, orbital (covalent) interactions remain as the likely reason. In such complexes these interactions are mainly manifested in the charge donation from nitrate oxygens to empty valence orbitals of the actinide. Most An 6d and 5f acceptor orbitals (and their hybrids) prefer non-linear arrangements for orbital interactions.

In order to understand the nature of orbital interactions in the $An^VO_2(NO_3)_2^-$ complexes, we performed a comparative analysis of the molecular orbitals in the D_{2h} and C_{2v} structures. The most characteristic orbitals of $Pu^VO_2(NO_3)_2^-$ (D_{2h}) and $Bk^VO_2(NO_3)_2^-$ (C_{2v}) from CASPT2 calculations are depicted in Figures 5 and 6, respectively.

The selected orbitals include the σ and π bonds of the AnO_2 moieties and a few molecular orbitals containing the interaction of An with the NO_3^- ligands. The latter donor-acceptor interactions are manifested in two π type interactions in the D_{2h} structure of $Pu^VO_2(NO_3)_2^-$. Both molecular orbitals have Pu 6d contributions. We note that mixing of 6d and 5f in these structures is not possible, because they belong to different irreducible representations of the D_{2h} point group.

In the C_{2v} structure of $Bk^VO_2(NO_3)_2^-$ four orbitals can be distinguished representing donor-acceptor interactions. All four interactions are of σ type operating within the plane of the nitrate ligands. In the first of these orbitals Bk interacts with four oxygens from the two nitrate ligands. In the three other orbitals the interaction is limited to one oxygen from each nitrate ligand. Because in the C_{2v} point group a mixing of 6d and 5f An orbitals (those which belong to the same irreducible representation) is possible, they can form 6d/5f hybrids. The hybrid formation facilitates a larger flexibility of the acceptor orbitals in the donor-acceptor interaction from both energetic and steric points of view.

Covalent bonding is an important issue in the chemistry of actinides. The possibility of separating minor actinides from lanthanides in spent nuclear fuel by appropriate heterocyclic organic ligands is attributed to the more covalent nature of actinide - ligand interactions with respect to the lanthanide - ligand ones. Numerous theoretical studies have been performed with the main goal of clarifying the electronic basis of the separation (see e.g. Refs. [40-53]). Less attention has been paid to the variation of covalency along the actinide row. Moreover, the different computed electronic parameters have led to controversial conclusions.

The early studies employed traditional tools of quantum chemistry such as charge and population analysis. Increasing covalency in solid AnO_2 towards the center of the 5f row was predicted by Prodan et al.[54] on the basis of spin densities (difference between alpha and beta electron densities) on the formally An^{IV} centers. The found increase of 5f spin density originates from a charge transfer from the oxygens, and as such, was assigned to covalent interactions.

For actinide complexes of the type $An[N(EPR_2)_2]_3$ (An = U-Cm; E = O, S, Se, Te; R = H, *i*-Pr, Ph), Kaltsoyannis et al. found also an increasing trend up to Am, with the largest 5f contribution in the metal-ligand bonding orbitals occurring in the Am complexes. However, instead of concluding on the highest covalency in the Am system, the authors attributed the large 5f contribution to an accidental energy match of the metal and ligand orbital energy levels.

This hypothesis was further elaborated in subsequent studies on $AnCp_3$ and $AnCp_4$ (Cp = η^5-C_5H_5) complexes across the 5f row from Th to Cm[55-57] by a joint analysis of the atomic charges, 5f spin densities, molecular orbitals and the electron and energy densities of the bond critical points (BCP, see atoms-in-molecules theory, AIM[58-59]). It was shown that the stabilization of the 5f orbitals across the actinide row results in an increased 5f population by charge transfer from the ligand to the An 5f orbitals, reaching the maximum at Am. This trend, however, does not appear in the density properties between the interacting atoms. From the point of view of orbital interactions the space between the bonding atoms is important. Here density properties can deviate from those localized on the atoms. The studies showed that the electron and energy densities at the BCPs decrease gradually from U to Cm, suggesting a decreasing covalency in the same direction. The same conclusion was drawn on the multiple AnN bond in terminal actinide nitride complexes, with the covalent character decreasing from An = U to Pu.[60] In contrast, in $AnO_2(H_2O)^+$ and $AnO(OH)_2^+$ cations the opposite trend, increasing from An = Pa to Pu, was suggested for the covalency of the An

oxygen bonds.[61] Such topological analysis has also been applied to other actinide compounds like actinocenes,[62-63] uranyl complexes,[64-66] and additional lanthanide and actinide compounds.[52, 67-70]

Of the various theoretical approaches only the AIM model can characterise quantitatively the space between the bonding atoms. Therefore we performed a topological analysis of the electron density distribution of the $An^{V}O_2(NO_3)_2^-$ complexes in order to see how the density properties of the An-O bonds vary along the 5f row. We were particularly interested in the parameters of An – nitrate interactions, as they may provide a clue on the increasing bend along the actinide row. A graphical representation of the bonding paths, bond and ring critical points of $Am^{V}O_2(NO_3)_2^-$ is shown in Figure 7.

Table 5. Selected computed results on the electron density distribution of $An^{V}O_2(NO_3)_2^-$ complexes and the dissociation energies.

Parameters[a]	Pu	Am	Cm	Bk	^{6}Cf	^{8}Cf
ρ(An-O_1)	0.298	0.291	0.262	0.257	0.258	0.196
ρ(An-O_2)	0.046	0.044	0.047	0.053	0.054	0.053
ρ(An-$O_{2'}$)	0.046	0.044	0.044	0.046	0.046	0.047
H(r)(An-O_1)	-0.254	-0.234	-0.185	-0.173	-0.177	-0.109
H(r)(An-O_2)	-0.0016	-0.0018	-0.0025	-0.0045	-0.0052	-0.0030
H(r)(An-$O_{2'}$)	-0.0016	-0.0018	-0.0017	-0.0019	-0.0024	-0.0049
δ(An,O_1)	1.92	1.93	1.78	1.67	1.66	1.61
δ(An,O_2)	0.26	0.24	0.26	0.29	0.29	0.27
δ(An,$O_{2'}$)	0.26	0.24	0.24	0.24	0.24	0.29
e(An)	+1.57	+1.60	+1.74	+1.90	+1.89	+2.02
e(O_1)	-0.54	-0.52	-0.59	-0.68	-0.67	-0.75
e(O_2)	-0.52	-0.54	-0.54	-0.54	-0.53	-0.55
e($O_{2'}$)	-0.52	-0.54	-0.54	-0.54	-0.54	-0.53
D_e	935.9	900.6	932.0	981.8	976.3	895.2[b]

[a]Computed at the B3LYP level. Electron density (ρ, a.u.) at the bond critical point (BCP) on the bond path between the indicated atoms; total electronic energy density [H(r), a.u.]; delocalization index, [δ(An,O), a.u.], atomic charges (e, a.u.) determined by Natural Bond Orbital analysis. The dissociation energy (D_e, kJ/mol) refers to the $An^{V}O_2(NO_3)_2^- = AnO_2^+ + 2NO_3^-$ reaction. The number in the upper left corner of Cf means the spin multiplicity.
[b]The dissociation energy to octet CfO_2^+ is 1149.9 kJ/mol.

Selected results of the topological analysis are given in Table 5. They include the electron density, ρ(r), and the total electronic energy density, H(r), at the An-O BCPs as well as the delocalization index, δ(An,O). The electron density at the BCP gives information on the magnitude of orbital overlap between the two atoms. Negative values of H(r) at the BCP mean significant electron sharing in the bonding, the magnitude being related to the covalence of the bonding. The delocalization index quantifies the average number of

electrons shared between two atoms, and as such can be considered as a quantitative measure of covalency.

Let's inspect first the actinyl (O_1-An-$O_{1'}$) bonds. The data in Table 5 indicate strong covalent contribution in these bonds: the values of ρ are generally greater than 0.2[59] and H(r) is in all the cases negative.[71] The decreasing magnitude of both parameters are in agreement with most previous conclusions on actinyl bonds, that the covalency decreases across the 5f series.[72] At the same time, the increasing ionic character in this direction is reflected in the increasing magnitudes of the NBO charges of An and O_1/$O_{1'}$.

The An - NO_3^- interaction is described by the BCPs between An and the two close-lying nitrate oxygens found in all the studied complexes. The small values of the BCP parameters listed in Table 5 confirm the weak character of An - ligand orbital interactions and that this bonding is mainly of ionic nature. We can observe a slight decrease in the electron density between Pu and Am, but from Am an increase can be clearly identified, particularly in the An-O_2 bond being shorter than An-$O_{2'}$. The above characteristics of the electron densities are supported by the H(r) data, their magnitudes increasing consistently from Am to Cf.

The most representative quantitative information on the covalent bonding is given by the delocalization index, δ(An,O). This parameter between N and O of a nitrate ligand is around 1.4 e in good agreement with the known bonding scenario of NO_3^-: it consists of one σ orbital for each N-O bond and a doubly occupied bonding π orbital delocalized over the NO_3 skeleton (the other four π valence electrons occupy non-bonding π orbitals). The actinyl AnO_1/$O_{1'}$ bonds are characterized by δ(An,O) values around 1.8 electron in good accordance with the strong covalent character of the actinyl bonds. The much weaker An – NO_3^- interactions have δ(An,O) values between 0.24-0.29 increasing from Am to Bk ≈ Cf, providing additional evidence for increasing covalency upon traversing this part of the actinide series.

Table 5 includes also the dissociation energies for the reaction $An^{V}O_2(NO_3)_2^- = AnO_2^+ + 2NO_3^-$. The Am complex has the smallest dissociation energy and it increases gradually towards Bk. This trend being parallel with the BCP parameters suggests that the covalent interactions have a major role in determining the stability trend of the $An^{V}O_2(NO_3)_2^-$ complexes. At the same time they explain the change of equilibrium structure from D_{2h} to C_{2v} in the section of the An row covered in the present study.

The increase of the dissociation energy of $An^{V}O_2(NO_3)_2^-$ across the An row is in agreement with observations that in solutions of An complexes, that of Cf showed larger binding constants than anticipated.[73] The feature was explained by the smaller size of the Cf ion relative to the lighter actinides, exerting a larger polarization on the electron density of the ligands. The larger polarization facilitates a larger charge transfer, i.e. stronger donor-acceptor interactions.

We note that $Cf^{V}O_2(NO_3)_2^-$ has slightly smaller dissociation energy than $Bk^{V}O_2(NO_3)_2^-$. This correlates well with the nearly identical values of the BCP parameters of these two complexes. It implies that the above discussed trends may not continue across the whole actinide row.

5. Relationships between oxidation states, reduction potentials, and ionization energies

Stabilities of oxidation states are indicated by standard reduction potentials that refer to aqueous solution but also have been found to effectively predict the existence of stable oxidation states in solids and gas-phase complexes.[74-75] The relationship between atomic properties and reduction potentials is illustrated by the IV/III reduction potential of metal ions, $E_0[M^{4+}/M^{3+}]$, which is the free energy for association of M^{4+} with an electron in aqueous solution, reaction 4 (where F is the Faraday constant). The electron affinity of a metal ion, $EA[M^{4+}]$, is also the energy for electron attachment but in this case for the free metal ion in vacuum rather than in solution. This EA can alternatively be expressed as the more commonly measured ionization energy according to reaction 5 where we employ the definition $IE[M^{3+}] \equiv EA[M^{4+}]$. The relationship between $E_0[M^{4+}/M^{3+}]$ and the gas-phase properties is given by equation 6 where $\Delta\Delta G_{solv}$ is the difference between solvation energies, $\Delta\Delta G_{solv} = \Delta G_{solv}[M^{3+}(aq)] - \Delta G_{solv}[M^{4+}(aq)]$, and E_{ref} is the reference electrode potential.[76]

$M^{4+}(aq) + e^- \rightarrow M^{3+}(aq)$ (4) $E_0[M^{4+}/M^{3+}] = -\Delta G^o/F$

$M^{4+}(g) + e^- \rightarrow M^{3+}(g)$ (5) $-\Delta E = EA[M^{4+}] \equiv IE[M^{3+}]$

$E_0[M^{4+}/M^{3+}] = IE[M^{3+}] - \Delta\Delta G_{solv} - E_{ref}$ (6)

The plot of $E_0[An^{4+}/An^{3+}]$ versus $IE[An^{3+}]$ in Fig. 8 for the actinides from Th through Cf exhibits a good correlation, except for An = U where $E_0[U^{4+}/U^{3+}]$ is well established but the assigned value of $IE[U^{3+}]$ is apparently significantly too high. Instead of the anomalously high literature value for $IE[U^{3+}]$ = 36.7 eV (diamond in Fig. 8), we adopt an estimate of $IE[U^{3+}]$ = 32.8 eV (encircled diamond in Fig. 8) to provide good inclusion of this point in the overall correlation. The linear correlation in Fig. 8 with a slope greater than unity (i.e. 1.276) indicates that the increase in $E_0[An^{4+}/An^{3+}]$ is diminished relative to that of $E[An^{3+}]$. This

suggests that $\Delta G_{solv}[An^{3+}]$ becomes less favorable relative to $\Delta G_{solv}[An^{4+}]$—i.e., $\Delta\Delta G_{solv}$ becomes increasingly positive—with increasing actinide atomic number. This trend is presumably a manifestation of the actinide contraction and indicates enhanced solvation free energy for An^{4+} versus An^{3+} with decreasing ionic radii.

The tetravalent oxidation state has been reported for the actinides from Th through Cf.[36] The relatively high $E_0[Es^{4+}/Es^{3+}]$ shown in Fig. 8 reveals the lower stability of Es(IV), an oxidation state that has not been definitively identified.[77] However, the estimated $E_0[Es^{4+}/Es^{3+}]$ (4.5 V)[7] is comparable to the corresponding reduction potentials for Nd^{4+} (4.6 V) and Dy^{4+} (5.0 V),[9] elements for which tetravalent oxidation state complexes are known;[78] it is thus likely that tetravalent Es should be similarly isolable. The IE$[An^{3+}]$ continue to increase beyond Es,[79] with a predicted concomitant increase in $E_0[An^{4+}/An^{3+}]$ and decreasing stability of the tetravalent oxidation states for the later An.

The above evaluation for IE$[An^{3+}]$ and $E_0[An^{4+}/An^{3+}]$ illustrates that there is generally a reliable correlation between gas-phase atomic ionization energies and condensed phase reduction potentials such that relative stabilities of oxidation states can be predicted, even though there may not be a corresponding quantitative variation in voltages for the two quantities—i.e., the slope may not be unity. The results in Figure 8 clearly and accurately predict from the relative values of IE$[An^{3+}]$ that the $An^{IV/III}$ reduction potentials should become more positive—i.e. reduction from An^{IV} to An^{III} becomes more favourable—upon traversing the actinide series from Th, where the Th^{IV} oxidation state is very stable, to Es, where the Es^{IV} oxidation state is not yet established. The demonstrated reliability of correlations such as this allows confident revision of IE$[U^{3+}]$ to provide consistency with the value of $E_0[U^{4+}/U^{3+}]$ that is well established. It is somewhat surprising that the previously assigned fourth ionization energy of the relatively common and well-studied actinide uranium, 36.7 eV, should evidently be in such substantial error relative to the revised estimate here of 32.8 eV. The value assigned in ref.[79] is from the ref.[80] where the following three values are cited: 36.7±1.0 eV;[81] 31.1 eV;[82] and 30.3 eV.[83] We conclude that the uncertainty assigned to the IE$[U^{3+}]$ of 36.7 eV, which was previously selected as the best value,[79-80] is actually significantly greater than ±1.0 eV, and that the actual IE$[U^{3+}]$ is closer to the reported lower value of 31.1 eV.[82]

For the nitrate complexes of particular interest here, reduction of pentavalent $[O=An^{V}=O]^{+}$, including in $AnO_2(NO_3)_2^-$, can occur by the following modifications to the actinyl(V) moiety: ***(i) reduction to An^{4+} concomitant with cleavage of the two An=O bonds;***

(ii) reduction to $[O=An^{IV}-O]^+$ with formally a double and a single actinide-oxo bond (or two intermediate-order bonds); or (iii) reduction to a $[An^{III}-(O_2)]^+$ peroxide with two single An-O bonds. In contrast to $An^{IV/III}$ reduction discussed above, conventional reduction of An^{V} to An^{IV} by process (i) does not correspond to simple charge reduction. For comparative purposes between actinides, the $An^{V/IV}$ reduction can be represented by reaction 7 in which the actinyl An=O bonds are cleaved during reduction. Formation of atomic oxygen as products in reaction 7 is arbitrary but does not affect *relative* reaction energetics for different actinides. Reaction 7 can be thermodynamically decomposed into bond cleavage reaction 8 and ionization reaction 9.

$AnO_2^+ \rightarrow An^{4+} + 2O + 3e^-$ (7)

$AnO_2^+ \rightarrow An^+ + 2O$ (8) $D[OAn^+-O] + D[An^+-O]$

$An^+ \rightarrow An^{4+} + 3e^-$ (9) $IE[An^+] + IE[An^{2+}] + IE[An^{3+}]$

The energies for reactions 8 and 9 for the actinides from Th through Cm are plotted in Figure 9. The aggregate bond dissociation energy for AnO_2^+, reaction 8, increases from ThO_2^+ to PaO_2^+, after which it monotonically decreases to CmO_2^+ (Fig. 9a).[84] The second component, the sum of the 2nd, 3rd and 4th IEs for reaction 9, increases from Th^+ to Am^+/Cm^+ (Fig. 9b).[79] The net result is that the energy for reaction 7 increases substantially from ThO_2^+ to PaO_2^+ to UO_2^+, after which it remains nearly constant, to within 1 eV, to CmO_2^+ (Fig. 9c). From the energies for reaction 7 it is predicted that the actinyl(V) ions from UO_2^+ to CmO_2^+ should exhibit similar stabilities towards dissociative reduction to An^{4+}. This assessment does not consider viability of synthesis of these AnO_2^+, or their potentially more facile alternative decomposition pathways such as by hydrolysis. The trend in stabilities of the $An^VO_2^+$ is accurately predicted, including for example that ThO_2^+ should be relatively unstable, which is largely a result of the high stability of Th^{4+} as is manifested by the low sum of ionization energies for Th^+ as plotted in Fig. 9b.

The intrinsic intramolecular rearrangement (not dissociative) actinyl(V) reductions assessed here computationally for the actinyl nitrates, and previously considered for bare actinyls,[10] are for processes (ii) and (iii) described above, which respectively correspond to (ii) reduction to An^{IV} by conversion of a double oxo-bond to a single oxo-bond, and (iii) reduction to An^{III} by conversion to two single bonds in a peroxide. Ionization energies for $[An^{3+}\rightarrow An^{4+}]$ (4th IE; the value employed for $IE[U^{3+}]$ is the corrected value derived here as discussed above), $[An^{4+}\rightarrow An^{5+}]$ (5th IE), and $[An^{3+}\rightarrow An^{5+}]$ (sum of 4th IE + 5th IE) are shown in Fig. 10. The 4th IEs exhibit an increase across the series, except for the incongruous

decrease from Cm^{3+} to Bk^{3+} that is a manifestation of the particular stability of the $5f^7$ half-filled shell of Bk^{4+}, an effect that also sustains the relatively prevalent Bk^{IV} oxidation state.[85]

The actinide 5th IEs (i.e., EA[An^{5+}]) provide an evaluation of the inherent propensity for the An^{5+} to reduce to An^{4+}. This process was computationally assessed here for $BkO_2(NO_3)_2^-$ and $CfO_2(NO_3)_2^-$ (see Table 3), with the result that for both Bk and Cf the conversion of An(V) to An(IV) is substantially endothermic. From the 5th ionization energies, 56.0±1.9 eV for Bk^{4+} and 51.9±1.9 eV for Cf^{4+},[79] it is predicted that the stability of Bk^V relative to Bk^{IV} should be lower than that of Cf^V relative to Cf^{IV}. Although the particularly stable $5f^7$ configuration of Bk^{4+} likely does result in IE[Bk^{4+}] > IE[Cf^{4+}], the large uncertainties in these ionization energies precludes quantitative comparisons of the relative stabilities of the Bk^V and Cf^V oxidation states based on the available IEs alone.

In previous work, the relative stabilities of $An^VO_2^+$ and $An^{IV}O_2^+$ were assessed for all An from Pa to Lr.[10] Only for the case of NoO_2^+ was the $An^{V/IV}$ reduction (ii) found to be exothermic and thus spontaneous. It is from this result that the approximate stability limit in Fig. 10b is assigned. Although reduction of $Th^VO_2^+$ to $Th^{IV}O_2^+$ was not evaluated, IE[Th^{4+}] corresponds to removal of an electron from the radon electronic core and should thus be sufficiently energetically demanding that the corresponding $Th^{V/IV}$ reduction is favorable, as suggested by placement of the estimated stability limit below Th^{5+} in Fig. 10b. A notable feature of the values plotted in Fig. 10b is that the assigned IE[No^{4+}] (60.0±1.9 eV) is higher than IE[Th^{4+}] (58.0±1.9 eV). Although an elevated IE[No^{4+}] is expected because this ionization corresponds to removal of two electrons from the closed-shell $5f^{14}$ configuration of No^{2+}, it would be remarkable if this process was more energetically demanding than ionization of the radon core of Th^{4+}. The seemingly anomalous phenomenon of IE[No^{4+}] > IE[Th^{4+}] could result from the expected general increase in ionization energy as atomic number increases, with the result being a substantial increase across the actinide series from IE[Pa^{4+}] to IE[Lr^{4+}], and possibly even a small increase from IE[Th^{4+}] to IE[No^{4+}]. However, the large uncertainties in these ionization energies indicate that this relative order is not fully established, and that it is feasible that IE[Th^{4+}] may actually be slightly higher than IE[No^{4+}]. A key point is that tetravalent $No^{IV}O_2^+$, and presumably also $Th^{IV}O_2^+$, are more stable than the hypothetical pentavalent species nobelyl(V) and thoryl(V).

From the results in Table 3 it is evident that both $Bk^{III}O_2(NO_3)_2^-$ and $Cf^{III}O_2(NO_3)_2^-$ are higher in energy than the corresponding $An^VO_2(NO_3)_2^-$. The previous assessment of bare dioxides similarly revealed the ground-state structures as $Bk^VO_2^+$ and $Cf^VO_2^+$.[10] Among the

other AnO_2^+, for An = Pa to Es the ground state is actinyl(V) except for $Cm^{III}O_2^+$, which is ~60 kJ/mol lower in energy than $Cm^{V}O_2^+$.[10] In contrast to bare $Cm^{III}O_2^+$ the identified ground state here is not $Cm^{III}O_2(NO_3)_2^-$ but rather $Cm^{V}O_2(NO_3)_2^-$. This disparity suggests that the energies of $Cm^{III}O_2^+$ and $Cm^{V}O_2^+$ are sufficiently similar that the relative energy ordering can be altered by the coordination environment, and specifically that coordinating nitrate anions can significantly stabilize Cm^V relative to Cm^{III} via electron donation to the curium center. A result of the particularly high IE[Lr^{3+}] due to its $5f^{14}$ closed shell is an oxidation state of Lr^{III} in both the peroxide and "lawrencyl(III)" dioxide structures of LrO_2^+. Another feature of the series of AnO_2^+ is ground state divalent superoxides for An = Fm, Md and No, which have the highest IE[An^{2+}] and are consequently specifically the actinides with stable divalent oxidation states.[7]

The evaluation here shows accord between stabilities of actinide oxidation states and the fundamental atomic property of ionization energy, which is known to correlate well with condensed phase reduction potentials, as is illustrated in Fig. 8. Of particular relevance here is the demonstration that An^{2+}-to-An^{3+}, An^{3+}-to-An^{4+} and An^{4+}-to-An^{5+} ionization energies can be employed to predict the stabilities of different oxidation states of bare and anion-coordinated AnO_2^+. Oxidation states An^{II}, An^{III}, An^{IV} and An^{V} in AnO_2^+ can result from altering the actinide-oxygen bonding to yield various combinations of An-O single, An=O double, and intermediate An···O bond orders, and from the absence or inclusion of direct oxygen-oxygen bonding. The predicted stable actinide oxidation state thus also predicts the nature of bonding and the structures of actinide dioxo cations. Although trends are similar for bare AnO_2^+ and the corresponding anion complexes $AnO_2(NO_3)_2^-$, the general expectation that coordination by anions should stabilize the higher An^V oxidation state is illustrated by the case of the ground-state $Cm^{V}O_2(NO_3)_2^-$ nitrate complex contrasting with bare $Cm^{III}O_2^+$.

Conclusions

Comparison of experimental results for lanthanide and actinide oxide nitrate anion complexes suggested the An^V oxidation state as coordinated actinyl(V) moieties embedded in $AnO_2(NO_3)_2^-$ for An = Pu, Am, Cm, Bk and Cf. The stability of oxidation state V in these $AnO_2(NO_3)_2^-$ complexes has been confirmed by quantum chemical calculations. The relative stability of this oxidation state is particularly notable for Cf and Bk complexes, therefore the $An^{IV}O_2(NO_3)_2^-$ and $An^{III}O_2(NO_3)_2^-$ forms have been explored and their lower stabilities with respect to Cf^V and Bk^V have been supported by both CASPT2 and DFT calculations. Whereas pentavalent Cf was expected to be stable due to a half-filled $5f^7$ configuration, the

computations show that this configuration for $Cf^{V}O_2(NO_3)_2^-$ is not octet with all seven 5f electrons spin-unpaired, but rather sextet with two of the 5f electrons spin-paired in a $5f_{1+}$ orbital.

The $AnO_2(NO_3)_2^-$ complexes show interesting bonding features. While in the actinyl moiety the ionic character of bonding increases from Pu to Cf (in agreement with experience on several other actinide systems), in the An – NO_3^- interaction an opposite trend has been observed here. The increasing ionicity in the AnO_2 moiety results in charge depletion around An making it more suitable as acceptor for charge transfer from the nitrate oxygens. The increasing covalent character from Pu to Bk ≈ Cf may be an important factor for the trend observed in the molecular geometries, i.e. a gradual bend of the NO_3^- ligands (described by the N-An-N angle) around An.

It is demonstrated that relevant ionization energies provide generally reliable assessments and predictions of the stabilities of both high and low oxidation states. This approach is particularly useful for the late actinides, and transactinides, for which condensed phase properties such as oxidation states and reduction potentials are generally inaccessible. It should be emphasized that many available ionization energies, even low IEs for relatively abundant and long-lived actinides such as U, remain as highly uncertain estimates. A priority should thus be to obtain by high level quantum computations more reliable ionization energies for actinides and transactinides, particularly IE[M^0] through IE[M^{7+}] that provide predictions of the viability of the oxidation states I to VIII that might be chemically relevant.

Acknowledgements

P.D.D. and J.K.G. were supported by the U.S. Department of Energy, Office of Basic Energy Sciences, Heavy Element Chemistry, at LBNL under Contract No. DE-AC02-05CH11231. The isotopes used in this research were supplied by the U.S. Department of Energy, Office of Science, by the Isotope Program in the Office of Nuclear Physics. The ^{249}Bk was provided to LBNL via the Isotope Development and Production for Research and Applications Program through the Radiochemical Engineering and Development Center at Oak Ridge National Laboratory. J.M. was supported by Fundação para a Ciência e a Tecnologia through projects PTDC/QEQ-QFI/6430/2014 and UID/Multi/04349/2013.

Supplementary Information

Computed geometrical parameters of $AnO_2(NO_3)_2^-$ complexes with penta-, tetra- and trivalent Cf and Bk obtained using the B3LYP exchange-correlation functional, and with tri- and tetravalent Cf and Bk obtained from CASPT2/DZ calculations. The related computed total

energies, Cartesian coordinates of the optimized structures, and frequencies and IR intensities (cm^{-1}, km/mol) of the vibrations of the AnO_2^+ moiety.

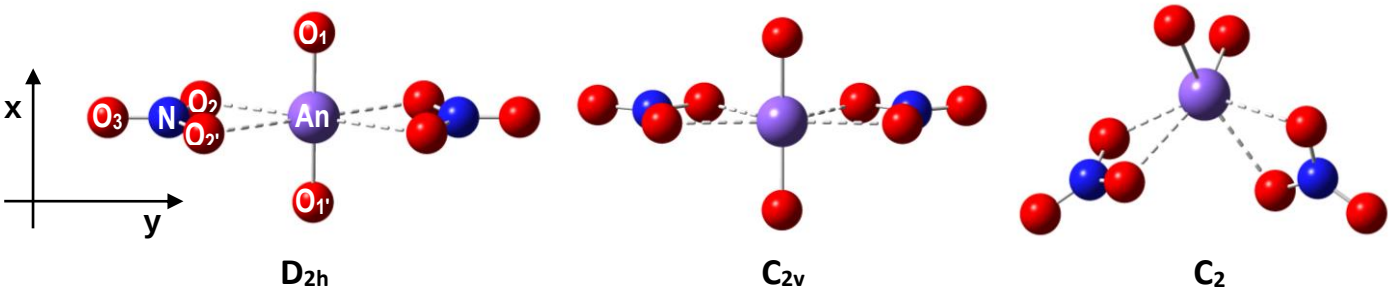

Scheme 1. Generic D_{2h}, C_{2v} and C_2 symmetry structures for $AnO_2(NO_3)_2^-$.

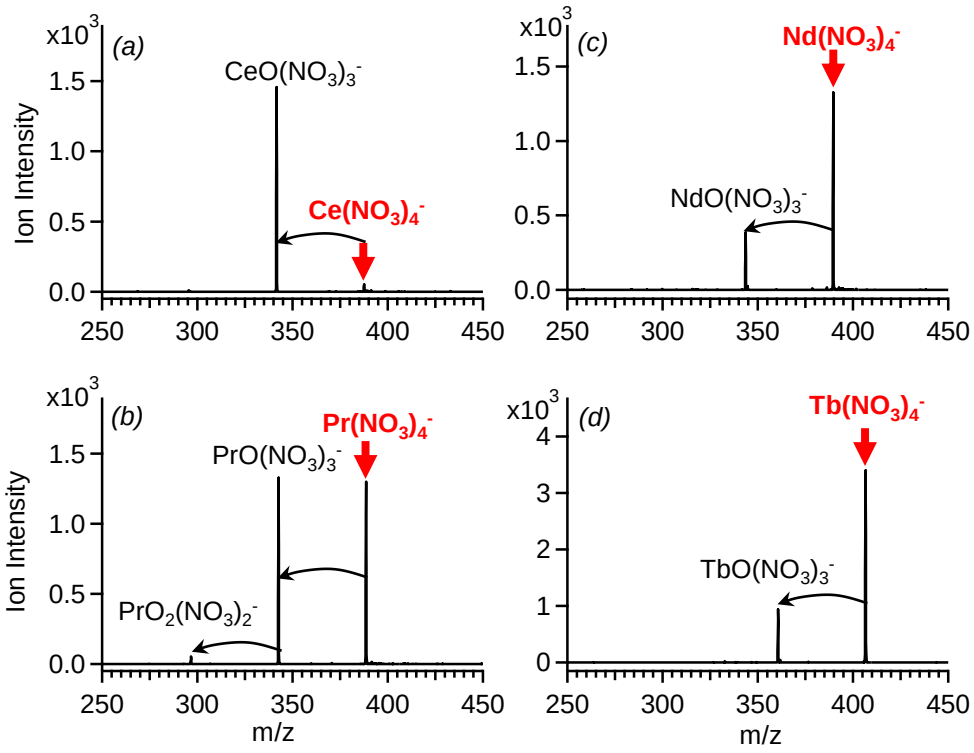

Figure 1. CID mass spectra acquired at a nominal instrumental voltage of 0.5 V for (a) $Ce(NO_3)_4^-$, (b) $Pr(NO_3)_4^-$, (c) $Nd(NO_3)_4^-$, and (d) $Tb(NO_3)_4^-$. Elimination of NO_2 is indicated by arrows. Sequential CID elimination of two NO_2 is observed only for $Pr(NO_3)_4^-$ to yield $PrO_2(NO_3)_2^-$.

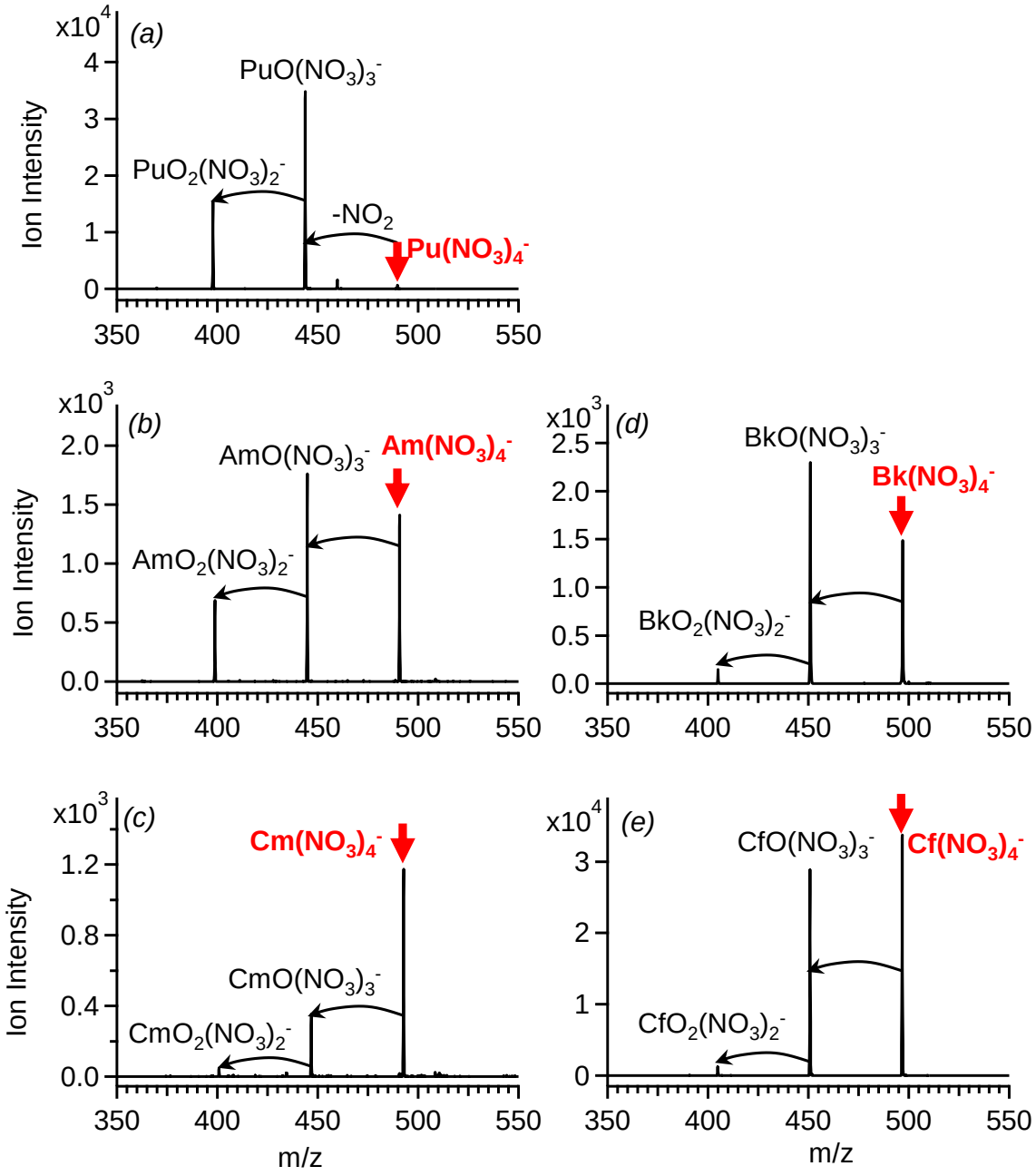

Figure 2. CID mass spectra acquired at a nominal instrumental voltage of 0.5 V for (a) $Pu(NO_3)_4^-$, (b) $Am(NO_3)_4^-$, (c) $Cm(NO_3)_4^-$, (d) $Bk(NO_3)_4^-$ (with 7% isobaric $Cf(NO_3)_4^-$ from beta-decay of ^{249}Bk) , and (e) $Cf(NO_3)_4^-$. Elimination of NO_2 is indicated by arrows. Sequential CID elimination of two NO_2 molecules from $An(NO_3)_4^-$ to yield $AnO_2(NO_3)_2^-$ is observed in all five cases.

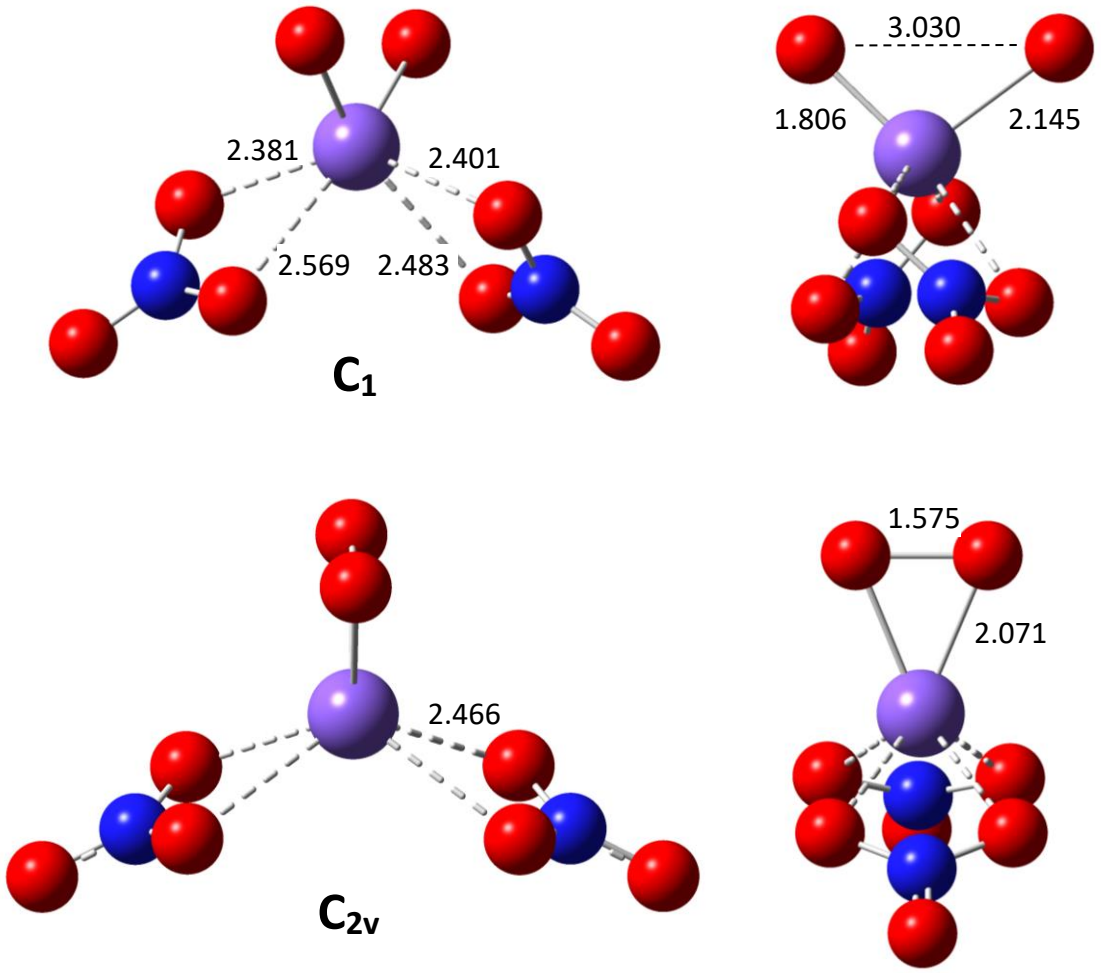

Figure 3. The structures of $Cf^{IV}O_2(NO_3)_2^-$ (top) and $Cf^{III}O_2(NO_3)_2^-$ (bottom) in two perspectives and selected distances in angstrom from CASPT2/DZ calculations.

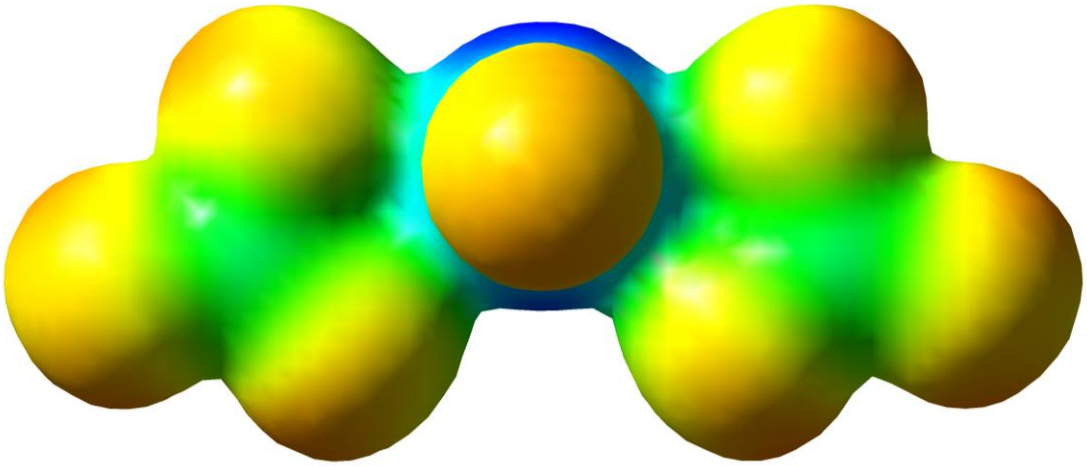

Figure 4. Electron density map of $CmO_2(NO_3)_2^-$ from DFT calculations. Charge concentration is indicated by yellow, while charge depletion by blue.

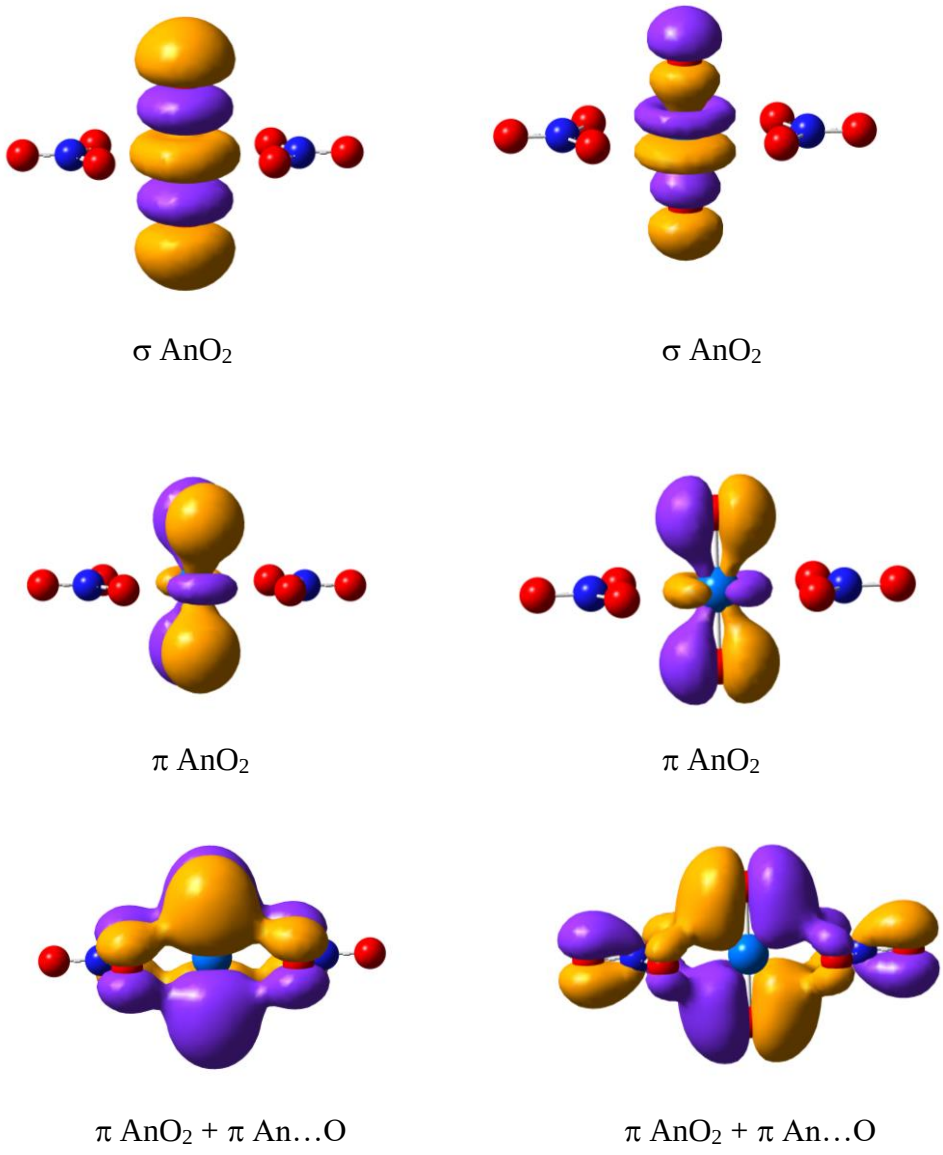

Figure 5. Characteristic molecular orbitals of $PuO_2(NO_3)_2^-$ from CASPT2 calculations.

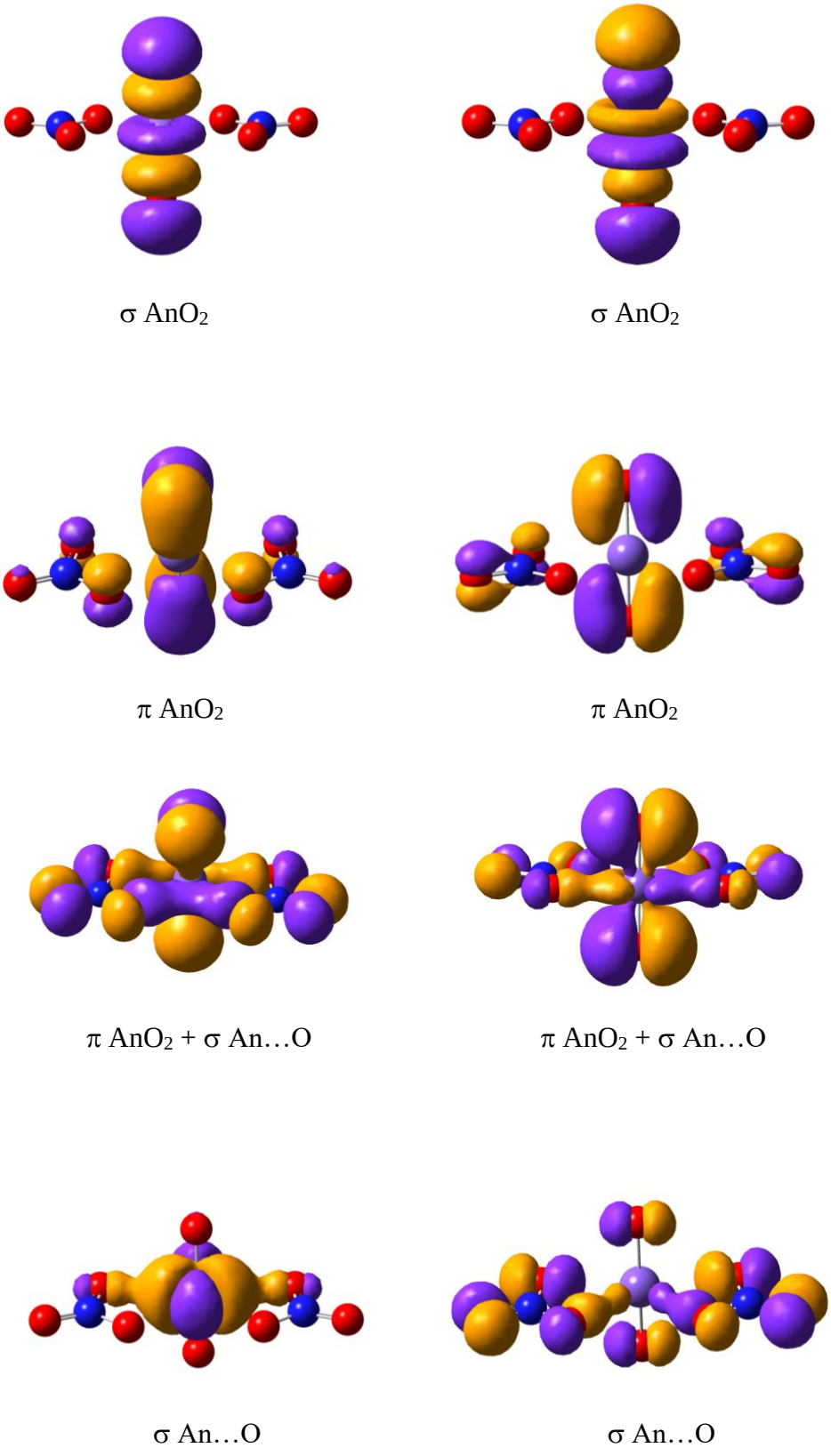

Figure 6. Characteristic molecular orbitals of $BkO_2(NO_3)_2^-$ from CASPT2 calculations.

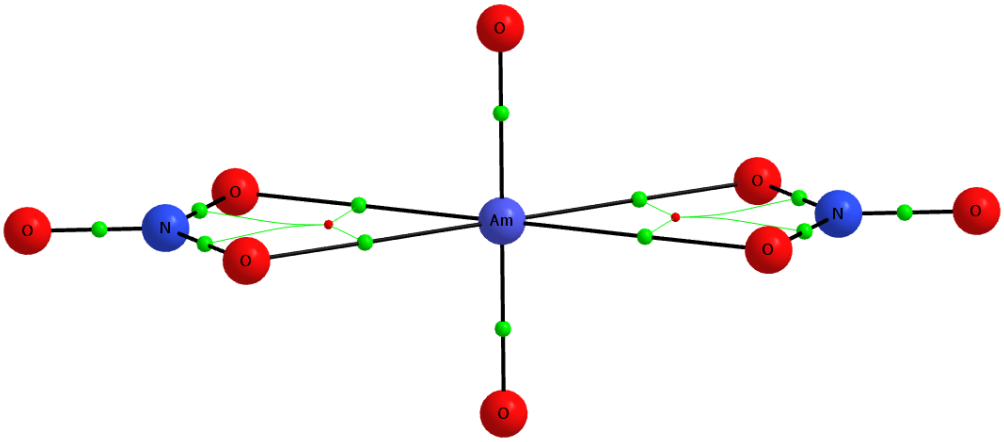

Figure 7. Bonding paths (black), bond (green) and ring (small red) critical points of $Am^{V}O_2(NO_3)_2^-$.

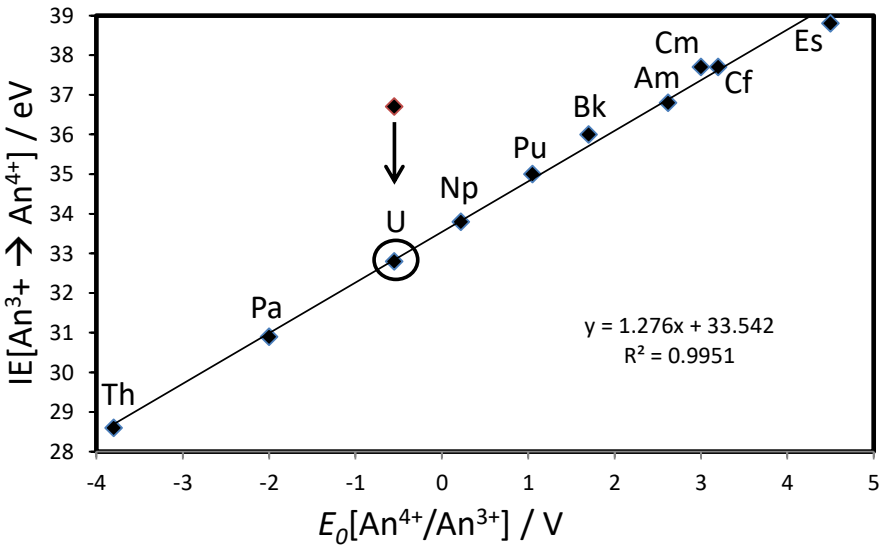

Figure 8. Plot of $E_0[An^{4+}/An^{3+}]$[7] versus IE[An^{3+}].[79] It is apparent that the reported IE[U^{3+}] (36.7 eV) is substantially too high; the new estimate plotted as the encircled point at 32.8 eV is assigned from the indicated linear correlation.

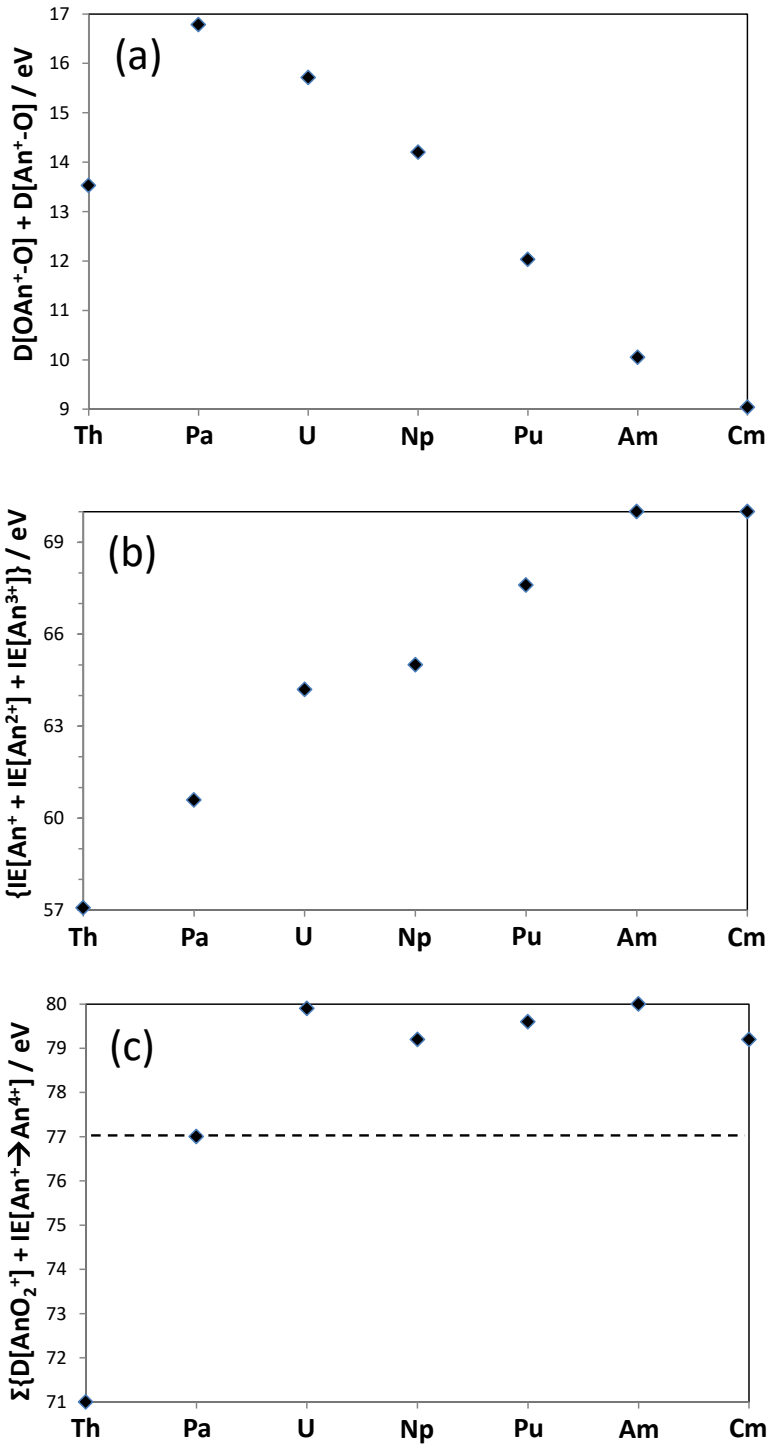

Figure 9. (a) Aggregate dissociation energy for AnO_2^+ to An^+ and 2O, i.e. reaction 8.[84] (b) Sum of 2nd, 3rd and 4th IEs, i.e. reaction 9. (c) Sum of energies in (a) and (b), i.e. reaction 7. Dotted line is approximate stability limit below which AnO_2^+ dissociatively reduces to An^{4+}.

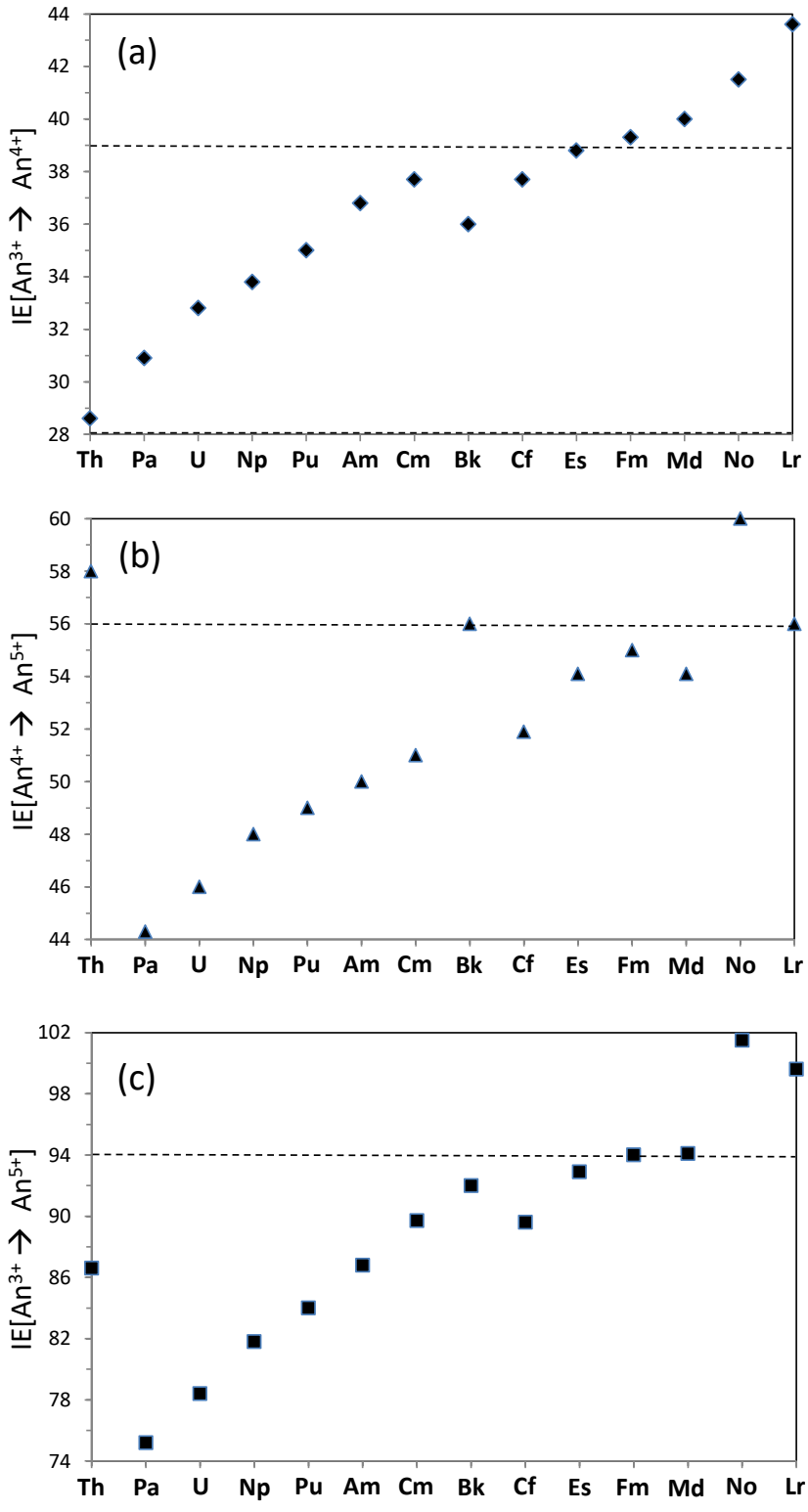

Figure 10. Actinide ionization energies in eV[79] (using corrected value for IE[U^{3+}] as discussed above): (a) 4th IE; (b) 5th IE; (c) Sum of 4th and 5th IEs. Dotted lines are approximate upper stability boundaries for: (a) An^{IV} relative to An^{III}; (b) An^{V} relative to An^{IV}; (c) An^{V} relative to An^{III}.

Table of Contents

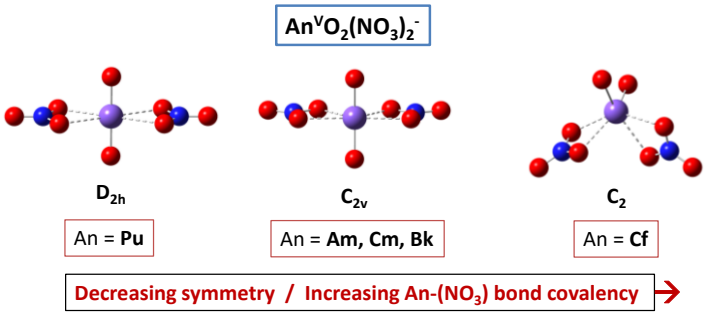

Synthesized gas-phase $AnO_2(NO_3)_2^-$ (An = Pu, Am, Cm, Bk, Cf) were computationally confirmed as actinyl(V) nitrates; this is the first Cm^V complex. Bonding analysis indicates increasing An-(NO_3) covalency from Pu to Cf, manifested as decreasing structural symmetry.

References

1. Wang, G. J.; Zhou, M. F.; Goettel, J. T.; Schrobilgen, G. J.; Su, J.; Li, J.; Schloder, T.; Riedel, S., Identification of an iridium-containing compound with a formal oxidation state of IX. *Nature* **2014,** *514* (7523), 475-478.
2. Yu, H. Y. S.; Truhlar, D. G., Oxidation State 10 Exists. *Angew. Chem. Int. Edit.* **2016,** *55* (31), 9004-9006.
3. Hu, S. X.; Li, W. L.; Lu, J. B.; Bao, J. L.; Yu, H. Y. S.; Truhlar, D. G.; Gibson, J. K.; Marçalo, J.; Zhou, M. F.; Riedel, S.; Schwarz, W. H. E.; Li, J., On the Upper Limits of Oxidation States in Chemistry. *Angew. Chem. Int. Edit.* **2018,** *57* (12), 3242-3245.
4. Santos, M.; de Matos, A. P.; Marçalo, J.; Gibson, J. K.; Haire, R. G.; Tyagi, R.; Pitzer, R. M., Oxidation of gas-phase protactinium ions, Pa(+) and Pa(2+): Formation and properties of PaO(2)(2+)(g), protactinyl. *J. Phys. Chem. A* **2006,** *110* (17), 5751-5759.
5. Zhang, Q. N.; Hu, S. X.; Qu, H.; Su, J.; Wang, G. J.; Lu, J. B.; Chen, M. H.; Zhou, M. F.; Li, J., Pentavalent Lanthanide Compounds: Formation and Characterization of Praseodymium(V) Oxides. *Angew. Chem. Int. Edit.* **2016,** *55* (24), 6896-6900.
6. Hu, S. X.; Jian, J. W.; Su, J.; Wu, X.; Li, J.; Zhou, M. F., Pentavalent lanthanide nitride-oxides: NPrO and NPrO- complexes with N equivalent to Pr triple bonds. *Chem. Sci.* **2017,** *8* (5), 4035-4043.
7. Edelstein, N. M.; Fuger, J.; Katz, J. J.; Morss, L. R., Summary and Comparison of the Properties of the Actinide and Transactinide Elements. In *The Chemistry of the Actinde and Transactinde Elements*, 3 ed.; Edelstein, N. M.; Fuger, J.; Morss, L. R., Eds. Springer: Dordrecht, 2006; Vol. 3, pp 1753-1835.
8. Silva, R. J., Fermium, Mendelevium, Nobelium, and Lawrencium. In *The Chemistry of the Actinde and Transactinde Elements*, Morss, L. R.; Edestein, N. M.; Fuger, J., Eds. Springer: Dordrecht, 2006; Vol. 3, pp 1621-1651.
9. Cotton, S., *Lanthanide and Actinde Chemistry*. John Wiley & Sons Ltd.: Chichester, 2006.
10. Dau, P. D.; Vasiliu, M.; Peterson, K. A.; Dixon, D. A.; Gibson, J. K., Remarkably High Stability of Late Actinide Dioxide Cations: Extending Chemistry to Pentavalent Berkelium and Californium. *Chem.-Eur. J.* **2017,** *23* (68), 17369-17378.
11. Runde, W. H.; Schulz, W. W., Americium. In *The Chemistry of the Actinide and Transactinide Elements*, 3 ed.; Morss, L. R.; Edelstein, N. M.; Fuger, J., Eds. Springer: Dordrecht, 2006; Vol. 2, pp 1265-1395.
12. Lucena, A. F.; Lourenço, C.; Michelini, M. C.; Rutkowski, P. X.; Carretas, J. M.; Zorz, N.; Berthon, L.; Dias, A.; Oliveira, M. C.; Gibson, J. K.; Marçalo, J., Synthesis and hydrolysis of gas-phase lanthanide and actinide oxide nitrate complexes: a correspondence to trivalent metal ion redox potentials and ionization energies. *Phys. Chem. Chem. Phys.* **2015,** *17* (15), 9942-9950.
13. Rios, D.; Rutkowski, P. X.; Shuh, D. K.; Bray, T. H.; Gibson, J. K.; Van Stipdonk, M. J., Electron transfer dissociation of dipositive uranyl and plutonyl coordination complexes. *J. Mass Spectrom.* **2011,** *46* (12), 1247-1254.
14. Rutkowski, P. X.; Michelini, M. C.; Bray, T. H.; Russo, N.; Marçalo, J.; Gibson, J. K., Hydration of gas-phase ytterbium ion complexes studied by experiment and theory. *Theor. Chem. Acc.* **2011,** *129* (3-5), 575-592.
15. Rios, D.; Michelini, M. C.; Lucena, A. F.; Marçalo, J.; Bray, T. H.; Gibson, J. K., Gas-Phase Uranyl, Neptunyl, and Plutonyl: Hydration and Oxidation Studied by Experiment and Theory. *Inorg. Chem.* **2012,** *51* (12), 6603-6614.
16. Frisch, M. J.; Trucks, G. W.; Schlegel, H. B.; Scuseria, G. E.; Robb, M. A.; Cheeseman, J. R.; Scalmani, G.; Barone, V.; Mennucci, B.; Petersson, G. A.; Nakatsuji, H.; Caricato, M.; Li, X.; Hratchian, H. P.; Izmaylov, A. F.; Bloino, J.; Zheng, G.; Sonnenberg, J. L.; Hada, M.; Ehara, M.; Toyota, K.; Fukuda,

R.; Hasegawa, J.; Ishida, M.; Nakajima, T.; Honda, Y.; Kitao, O.; Nakai, H.; Vreven, T.; Montgomery Jr., J. A.; Peralta, J. E.; Ogliaro, F.; Bearpark, M.; Heyd, J. J.; Brothers, E.; Kudin, K. N.; Staroverov, V. N.; Keith, T.; Kobayashi, R.; Normand, J.; Raghavachari, K.; Rendell, A.; Burant, J. C.; Iyengar, S. S.; Tomasi, J.; Cossi, M.; Rega, N.; Millam, J. M.; Klene, M.; Knox, J. E.; Cross, J. B.; Bakken, V.; Adamo, C.; Jaramillo, J.; Gomperts, R.; Stratmann, R. E.; Yazyev, O.; Austin, A. J.; Cammi, R.; Pomelli, C.; Ochterski, J. W.; Martin, R. L.; Morokuma, K.; Zakrzewski, V. G.; Voth, G. A.; Salvador, P.; Dannenberg, J. J.; Dapprich, S.; Daniels, A. D.; Farkas, O.; Foresman, J. B.; Ortiz, J. V.; Cioslowski, J.; Fox, D. J. *Gaussian 09, Revision D.01*, Gaussian, Inc.: Wallingford CT, 2010.

17. Becke, A. D., Density-Functional Thermochemistry. III. The Role of Exact Exchange. *J. Chem. Phys.* **1993,** *98*, 5648-5652.

18. Lee, C.; Yang, W.; Parr, R. G., Development of the Colle-Salvetti Correlation-Energy Formula into a Functional of the Electron Density. *Phys. Rev. B* **1988,** *37*, 785-789.

19. Küchle, W.; Dolg, M.; Stoll, H.; Preuss, H., Energy-Adjusted Pseudopotentials for the Actinides. Parameter Sets and Test Calculations for Thorium and Thorium Monoxide. *J. Chem. Phys.* **1994,** *100* (10), 7535-7542.

20. Cao, X.; Dolg, M.; Stoll, H., Valence basis sets for relativistic energy-consistent small-core actinide pseudopotentials. *J. Chem. Phys.* **2003,** *118*, 487-496.

21. Dunning Jr., T. H., Gaussian basis sets for use in correlated molecular calculations. I. The atoms boron through neon and hydrogen. *J. Chem. Phys.* **1989,** *90*, 1007-1023.

22. Kendall, R. A.; Dunning Jr., T. H.; Harrison, R. J., Electron Affinities of the First-Row Atoms Revisited. Systematic Basis Sets and Wave Functions. *J. Chem. Phys.* **1992,** *96*, 6796-6806.

23. Keith, T. A. *AIMAll (Version 17.11.14)*, TK Gristmill Software, Overland Park KS, USA: 2017.

24. Reed, A. E.; Curtiss, L. A.; Weinhold, F., Intermolecular interactions from a natural bond orbital, donor-acceptor viewpoint. *Chem. Rev.* **1988,** *88*, 899-926.

25. Glendening, E. D.; Badenhoop, J. K.; Reed, A. E.; Carpenter, J. E.; Bohmann, J. A.; Morales, C. M.; Weinhold, F. *NBO 5.9*, Theoretical Chemistry Institute, University of Wisconsin: Madison, US, 2011.

26. Karlström, G.; Lindh, R.; Malmqvist, P.-Å.; Roos, B. O.; Ryde, U.; Veryazov, V.; Widmark, P.-O.; Cossi, M.; Schimmelpfennig, B.; Neogrady, P.; Seijo, L., MOLCAS: A Program Package for Computational Chemistry. *Comput. Mat. Sci.* **2003,** *28*, 222-239.

27. Aquilante, F.; Autschbach, J.; Carlson, R. K.; Chibotaru, L. F.; Delcey, M. G.; De Vico, L.; Galván, I. F.; Ferré, N.; Frutos, L. M.; Gagliardi, L.; Garavelli, M.; Giussani, A.; Hoyer, C. E.; Li Manni, G.; Lischka, H.; Ma, D.; Malmqvist, P. Å.; Müller, T.; Nenov, A.; Olivucci, M.; Pedersen, T. B.; Peng, D.; Plasser, F.; Pritchard, B.; Reiher, M.; Rivalta, I.; Schapiro, I.; Segarra-Martí, J.; Stenrup, M.; Truhlar, D. G.; Ungur, L.; Valentini, A.; Vancoillie, S.; Veryazov, V.; Vysotskiy, V. P.; Weingart, O.; Zapata, F.; Lindh, R., MOLCAS 8: New Capabilities for Multiconfigurational Quantum Chemical Calculations Across the Periodic Table. *J. Comput. Chem.* **2016,** *37*, 506-541.

28. Roos, B. O., In *Advances in Chemical Physics, Ab Initio Methods in Quantum Chemistry - II*, Lawley, K. P., Ed. John Wiley & Sons Ltd.: Chichester, 1987; pp 399-446.

29. Andersson, K.; Malmqvist, P.-Å.; Roos, B. O.; Sadlej, A.; Wolinski, K., Second-Order Perturbation Theory with a CASSCF Reference Function. *J. Phys. Chem.* **1990,** *94*, 5483-5488.

30. Andersson, K.; Malmqvist, P.-Å.; Roos, B. O., Second-Order Perturbation Theory with a Complete Active Space Self-Consistent Field Reference Function. *J. Chem. Phys.* **1992,** *96*, 1218-1226.

31. Douglas, N.; Kroll, N. M., Quantum Electrodynamical Corrections to the Fine Structure of Helium. *Ann. Phys.* **1974,** *82* (1), 89-155.

32. Hess, B. A., Relativistic Electronic-Structure Calculations Employing a Two-Component No-Pair Formalism with External-Field Projection Operators. *Phys. Rev. A* **1986,** *33* (6), 3742-3748.

33. Roos, B. O.; Lindh, R.; Malmqvist, P.-Å.; Veryazov, V.; Widmark, P.-O., New Relativistic ANO Basis Sets for Actinide Atoms. *Chem. Phys. Lett.* **2005,** *409*, 295-299.

34. Roos, B. O.; Lindh, R.; Malmqvist, P.-Å.; Veryazov, V.; Widmark, P.-O., Main Group Atoms and Dimers Studied with a New Relativistic ANO Basis Set. *J. Phys. Chem. A* **2004,** *108*, 2851-2858.
35. Veryazov, V.; Malmqvist, P. Å.; Roos, B. O., How to Select Active Space for Multiconfigurational Quantum Chemistry? *Int. J. Quantum. Chem.* **2011,** *111*, 3329-3338.
36. Morss, L. R.; Edelstein, N. M.; Fuger, J., *The Chemistry of the Actinide and Transactinide Elements*. 3 ed.; Springer: Dordrecht, 2006.
37. Kovács, A., Relativistic Multireference Quantum Chemical Study of the Electronic Structure of Actinide Trioxide Molecules. *J. Phys. Chem. A* **2017**.
38. Kovács, A.; Konings, R. J. M.; Gibson, J. K.; Infante, I.; Gagliardi, L., Quantum Chemical Calculations and Experimental Investigations of Molecular Actinide Oxides. *Chem. Rev.* **2015,** *115*, 1725-1759.
39. Infante, I.; Kovács, A.; La Macchia, G.; Shahi, A. R. M.; Gibson, J. K.; Gagliardi, L., Ionization Energies for the Actinide Mono- and Dioxides Series, from Th to Cm: Theory versus Experiment. *J. Phys. Chem. A* **2010,** *114* (19), 6007-6015.
40. Strittmatter, R. J.; Bursten, B. E., Bonding in tris(η5-cyclopentadienyl) actinide complexes. 5. A comparison of the bonding in Np, Pu, and transplutonium compounds with that in lanthanide compounds and a transition-metal analogue. *J. Am. Chem. Soc.* **1991,** *113* (2), 552-559.
41. Choppin, G. R., Covalency in f-element bonds. *J. Alloys Comp.* **2002,** *344* (1-2), 55-59.
42. Denecke, M. A.; Rossberg, A.; Panak, P. J.; Weigl, M.; Schimmelpfennig, B.; Geist, A., Characterization and comparison of Cm(III) and Eu(III) complexed with 2,6-di(5,6-dipropyl-1,2,4-triazin-3-yl)pyridine using EXAFS, TRFLS, and quantum-chemical methods. *Inorg. Chem.* **2005,** *44* (23), 8418-8425.
43. Guillaumont, D., Quantum Chemistry Study of Actinide(III) and Lanthanide(III) Complexes with Tridentate Nitrogen Ligands. *J. Phys. Chem. A* **2004,** *108*, 6893-6900.
44. Miguirditchian, M.; Guillaneux, D.; Guillaumont, D.; Moisy, P.; Madic, C.; Jensen, M. P.; Nash, K. L., Thermodynamic study of the complexation of trivalent actinide and lanthanide cations by ADPTZ, a tridentate N-donor ligand. *Inorg. Chem.* **2005,** *44* (5), 1404-1412.
45. Gaunt, A. J.; Reilly, S. D.; Enriquez, A. E.; Scott, B. L.; Ibers, J. A.; Sekar, P.; Ingram, K. I. M.; Kaltsoyannis, N.; Neu, M. P., Experimental and theoretical comparison of actinide and lanthanide bonding in $M[N(EPR_2)_2]_3$ complexes (M = U, Pu, La, Ce; E = S, Se, Te; R = Ph, iPr, H). *Inorg. Chem.* **2008,** *47* (1), 29-41.
46. Meskaldji, S.; Belkhiri, L.; Arliguie, T.; Fourmigué, M.; Ephritikhine, M.; Boucekkine, A., Density functional theory investigations of the homoleptic tris(dithiolene) complexes $[M(dddt)_3]$-q (q=3, 2; M = Nd^{3+} and $U^{3+/4+}$) related to lanthanide(lll)/actinide(lll) differentiation. *Inorg. Chem.* **2010,** *49* (7), 3192-3200.
47. Arnold, P. L.; Turner, Z. R.; Kaltsoyannis, N.; Pelekanaki, P.; Bellabarba, R. M.; Tooze, R. P., Covalency in Ce^{IV} and U^{IV} halide and N-heterocyclic carbene bonds. *Chem. Eur. J.* **2010,** *16* (31), 9623-9629.
48. Lan, J.-H.; Shi, W.-Q.; Yuan, L.-Y.; Li, J.; Zhao, Y.-L.; Chai, Z.-F., Recent advances in computational modeling and simulations on the An(III)/Ln(III) separation process. *Coord. Chem. Rev.* **2012,** *256* (13-14), 1406-1417.
49. Hancock, R. D.; Bartolotti, L. J., A DFT study of the affinity of lanthanide and actinide ions for sulfur-donor and nitrogen-donor ligands in aqueous solution. *Inorg. Chim. Acta* **2013,** *396*, 101-107.
50. Jones, M. B.; Gaunt, A. J.; Gordon, J. C.; Kaltsoyannis, N.; Neu, M. P.; Scott, B. L., Uncovering f-element bonding differences and electronic structure in a series of 1:3 and 1:4 complexes with a diselenophosphinate ligand. *Chem. Sci.* **2013,** *4* (3), 1189-1203.
51. Narbutt, J.; Wodyński, A.; Pecul, M., The selectivity of diglycolamide (TODGA) and bis-triazine-bipyridine (BTBP) ligands in actinide/lanthanide complexation and solvent extraction separation-a theoretical approach. *Dalton Trans.* **2015,** *44* (6), 2657-2666.

52. Fryer-Kanssen, I.; Austin, J.; Kerridge, A., Topological Study of Bonding in Aquo and Bis(triazinyl)pyridine Complexes of Trivalent Lanthanides and Actinides: Does Covalency Imply Stability? *Inorg. Chem.* **2016,** *55* (20), 10034-10042.
53. Trumm, M.; Schimmelpfennig, B., Towards the origin of effective An(III)/Ln(III) separation by tridentate N-donor ligands: A theoretical study on atomic charges and polarisabilities for Cm(III)/Gd(III) separation. *Mol. Phys.* **2016,** *114* (6), 876-883.
54. Prodan, I. D.; Scuseria, G. E.; Martin, R. L., Covalency in the actinide dioxides: Systematic study of the electronic properties using screened hybrid density functional theory. *Phys. Rev. B* **2007,** *76* (3), 033101.
55. Tassell, M. J.; Kaltsoyannis, N., Covalency in $AnCp_4$ (An = Th–Cm): a comparison of molecular orbital, natural population and atoms-in-molecules analyses. *Dalton Trans.* **2010,** *39* (29), 6719-6725.
56. Kirker, I.; Kaltsoyannis, N., Does covalency really increase across the 5f series? A comparison of molecular orbital, natural population, spin and electron density analyses of $AnCp_3$ (An = Th- Cm, Cp = η^5-C_5H_5). *Dalton Trans.* **2011,** *40*, 124-131.
57. Kaltsoyannis, N., Does Covalency Increase or Decrease across the Actinide Series? Implications for Minor Actinide Partitioning. *Inorg. Chem.* **2013,** *52*, 3407−3413.
58. Bader, R. F. W., *Atoms in Molecules. A Quantum Theory*. Oxford University Press: Oxford, 1990.
59. Matta, C. F.; Boyd, R. J., In *The Quantum Theory of Atoms in Molecules*, Matta, C. F.; Boyd, R. J., Eds. Wiley-VCH: Weinheim, 2007; pp 1-34.
60. Wu, Q.-Y.; Wang, C.-Z.; Lan, J.-H.; Xiao, C.-L.; Wang, X.-K.; Zhao, Y.-L.; Chai, Z.-F.; Shi, W.-Q., Theoretical Investigation on Multiple Bonds in Terminal Actinide Nitride Complexes. *Inorg. Chem.* **2014,** *53*, 9607−9614.
61. Kaltsoyannis, N., Covalency hinders $AnO_2(H_2O)^+ \rightarrow AnO(OH)_2^+$ isomerisation (An = Pa–Pu). *Dalton Trans.* **2016,** *45*, 3158-3162.
62. Kerridge, A., Oxidation state and covalency in f-element metallocenes (M = Ce, Th, Pu): A combined CASSCF and topological study. *Dalton Trans.* **2013,** *42* (46), 16428-16436.
63. Kerridge, A., f-Orbital covalency in the actinocenes (An = Th–Cm): multiconfigurational studies and topological analysis. *RSC Adv.* **2014,** *4*, 12078-12086.
64. Di Pietro, P.; Kerridge, A., U-O_{yl} Stretching Vibrations as a Quantitative Measure of the Equatorial Bond Covalency in Uranyl Complexes: A Quantum-Chemical Investigation. *Inorg. Chem.* **2016,** *55* (2), 573-583.
65. Di Pietro, P.; Kerridge, A., Assessing covalency in equatorial U-N bonds: Density based measures of bonding in BTP and isoamethyrin complexes of uranyl. *Phys. Chem. Chem. Phys.* **2016,** *18* (25), 16830-16839.
66. Di Pietro, P.; Kerridge, A., Ligand size dependence of U-N and U-O bond character in a series of uranyl hexaphyrin complexes: Quantum chemical simulation and density based analysis. *Phys. Chem. Chem. Phys.* **2017,** *19* (11), 7546-7559.
67. Beekmeyer, R.; Kerridge, A., Assessing Covalency in Cerium and Uranium Hexachlorides: A Correlated Wavefunction and Density Functional Theory Study. *Inorganics* **2015,** *3* (4), 482-499.
68. Gregson, M.; Lu, E.; Tuna, F.; McInnes, E. J. L.; Hennig, C.; Scheinost, A. C.; McMaster, J.; Lewis, W.; Blake, A. J.; Kerridge, A.; Liddle, S. T., Emergence of comparable covalency in isostructural cerium(IV)- and uranium(IV)-carbon multiple bonds. *Chem. Sci.* **2016,** *7* (5), 3286-3297.
69. Gregson, M.; Lu, E.; Mills, D. P.; Tuna, F.; McInnes, E. J. L.; Hennig, C.; Scheinost, A. C.; McMaster, J.; Lewis, W.; Blake, A. J.; Kerridge, A.; Liddle, S. T., The inverse-trans-influence in tetravalent lanthanide and actinide bis(carbene) complexes. *Nature Communications* **2017,** *8*, 14137.
70. Kerridge, A., Quantification of f-element covalency through analysis of the electron density: insights from simulation. *Chem. Commun.* **2017,** *53*, 6685-6695.

71. Cremer, D.; Kraka, E., Chemical Bonds without Bonding Electron Density — Does the Difference Electron-Density Analysis Suffice for a Description of the Chemical Bond? *Angew. Chem. Int. Ed.* **1984,** *23* (8), 627-628.
72. Kaltsoyannis, N.; Scott, P., *The f elements*. Oxford University Press: Oxford, 1999.
73. Choppin, G. R.; Jensen, M. P., Actinides in Solution: Complexation and Kinetics. In *The Chemistry of the Actinide and Transactinide Elements*, Morss, L. R.; Edelstein, N. M.; Fuger, J., Eds. Springer: Dordrecht, 2006; Vol. 4, pp 2574–2575.
74. Yagi, S.; Nakanishi, H.; Ichitsubo, T.; Matsubara, E., Oxidation-State Control of Nanoparticles Synthesized via Chemical Reduction Using Potential Diagrams. *J. Electrochem. Soc.* **2009,** *156* (8), D321-D325.
75. Gong, Y.; Tian, G. X.; Rao, L. F.; Gibson, J. K., Dissociation of Diglycolamide Complexes of Ln(3+) (Ln = La-Lu) and An(3+) (An = Pu, Am, Cm): Redox Chemistry of 4f and 5f Elements in the Gas Phase Parallels Solution Behavior. *Inorg. Chem.* **2014,** *53* (22), 12135-12140.
76. Calbo, J.; Viruela, R.; Orti, E.; Arago, J., Relationship between Electron Affinity and Half-Wave Reduction Potential: A Theoretical Study on Cyclic Electron-Acceptor Compounds. *ChemPhysChem* **2016,** *17* (23), 3881-3890.
77. Haire, R. G., Einsteinium. In *The Chemistry of the Actinide and Transactinide Elements*, Morss, L. R.; Edestein, N. M.; Fuger, J., Eds. Springer: Dordrecht, 2006; Vol. 3, pp 1577-1620.
78. Varga, L. P.; Asprey, L. B., Electronic Spectra of Weak-Field Fluoride Complexes of Tetravalent Neodymium. *J. Chem. Phys.* **1968,** *49* (10), 4674-4679.
79. Kramida, A.; Ralchenko, Y.; Reader, J. NIST Atomic Spectra Database (https://physics.nist.gov/cgi-bin/ASD/ie.pl). https://physics.nist.gov.
80. Blaise, J.; Wyart, J.-F., *International Tables of Selected Constants*. Centre National de lar Recherche Scientifique: Paris, 1992; Vol. 20.
81. Emel'yanov, A. M.; Khodeev, Y. S.; Gorokhov, L. N., *Teplofiz. vysokikh Temp. S.S.S.R.* **1970,** *8*, 508-513.
82. Thomson, S. L.; Lauson, H. S. *Report SC-RR-710713*; Sandia Laboratory: Albuquerque, NM, 1972.
83. Rashid, K.; Saadi, M. Z.; Yasin, M., Dirac Fock Total Energies, Ionization Energies, and Orbital Energies for Uranium Ions U-I to U-XCII. *Atom. Data Nucl. Data* **1988,** *40* (2), 365-378.
84. Marçalo, J.; Gibson, J. K., Gas-Phase Energetics of Actinide Oxides: An Assessment of Neutral and Cationic Monoxides and Dioxides from Thorium to Curium. *J. Phys. Chem. A* **2009,** *113* (45), 12599-12606.
85. Hobart, D. E.; Peterson, J. R., Berkelium. In *The Chemistry of the Actinide and Transactinide Elements*, Morss, L. R.; Edeslstein, N. M.; Fuger, J., Eds. Springer: Dordrecht, 2006; Vol. 3, pp 1444-1498.